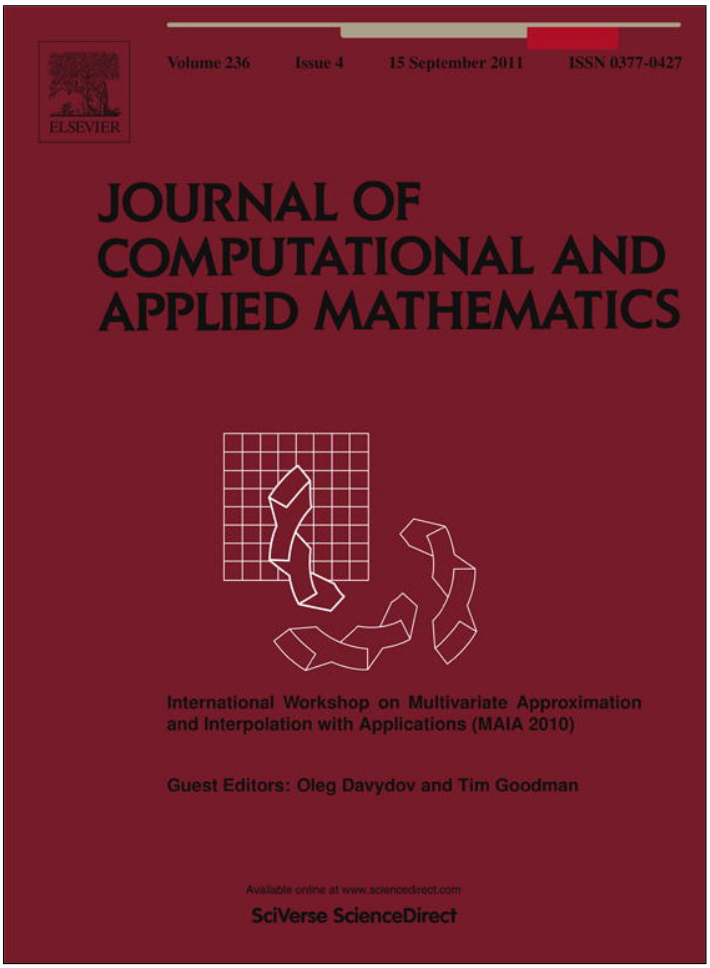

Journal of Computational and Applied Mathematics 236 (2011) 511–528

Contents lists available at SciVerse ScienceDirect

Journal of Computational and Applied Mathematics

journal homepage: www.elsevier.com/locate/cam

Isogeometric analysis in advection–diffusion problems: Tension splines approximation

Carla Manni [a,*], Francesca Pelosi [a], M. Lucia Sampoli [b]

[a] Dipartimento di Matematica, Università di Roma "Tor Vergata", Italy

[b] Dipartimento di Scienze Matematiche ed Informatiche, Università di Siena, Italy

ARTICLE INFO

Keywords:
Advection–diffusion problems
Isogeometric Analysis
Variable degree splines
Exponential splines
Splines in tension

ABSTRACT

We present a novel approach, within the new paradigm of isogeometric analysis introduced by Hughes et al. (2005) [6], to deal with advection dominated advection–diffusion problems. The key ingredient is the use of Galerkin approximating spaces of functions with high smoothness, as in IgA based on classical B-splines, but particularly well suited to describe sharp layers involving very strong gradients.

1. Introduction

The advection–diffusion equation governs several important phenomena in physics and engineering, and it is the basis of advanced fluid problems such as Navier–Stokes problems. Therefore it has been the focus of intense research for quite some time (see e.g., [1–4] and references therein).

The fluid equations are fundamentally different than the structural equations in that advection dominated flow phenomena are characterized by essentially skew-symmetric differential operators, instead of the symmetric operators which characterize typical structural analysis models. Another complicated flow feature is sharp layers involving very strong gradients where diffusive behavior prevails. As a consequence, successful fluid analysis formulations need to automatically account for the local competition between advective and diffusive effects. The standard Galerkin formulation optimally deals with symmetric-definite operators but produces unstable discretizations of skew-symmetric operators. Indeed classical numerical methods based on the standard Galerkin finite element approach lack stability and this manifests itself in terms of nonphysical oscillations.

In order to correct the deficiencies in the standard Galerkin approach, Hughes and coauthors introduced the streamline upwind Petrov–Galerkin (SUPG) technique, [1]. This technique turned out to be the forerunner of a new class of stabilization schemes, called the Galerkin/least-square (GLS) stabilization methods, [5]. In the context of the advection–diffusion equation, the essential feature of these methods is the stabilization of the advection operator without upsetting consistency or compromising accuracy.

With the introduction of the new paradigm given by the isogeometric analysis, in [6] the ability of the isogeometric approach, in conjunction with SUPG, to solve challenging test cases for the advection–diffusion equation was investigated, see also [7–9]. Isogeometric analysis is basically a higher-order approach and therefore we cannot expect a better behavior with respect to the extraneous oscillations. The Gibbs phenomena noted for polynomial-based finite element methods tend to become more pronounced as the polynomial order is increased. However, as noted in [6], the variation diminishing property of the Dirichlet boundary condition specification, plus the notion of k-refinement, that is the use of high order piecewise polynomials (rationals) with maximal global smoothness, leads to some remarkable results in the case of NURBS.

* Corresponding author. Tel.: +39 05572594660.
E-mail addresses: manni@mat.uniroma2.it (C. Manni), pelosi@mat.uniroma2.it (F. Pelosi), sampoli@unisi.it (M.L. Sampoli).

0377-0427/$ – see front matter © 2011 Elsevier B.V. All rights reserved.
doi:10.1016/j.cam.2011.05.029

The aim of this paper is to show how this last approach can be improved using, instead of NURBS or B-splines, suitable generalizations of classical B-splines, able to describe sharp variations. These classes of splines belong to the so called tensioned splines, which have the additional feature of reducing as much as possible extraneous oscillations. In particular, we focus on exponential and variable degree B-splines.

As illustrated by several numerical tests, the use of exponential and variable degree splines in the context of IgA for advection dominated advective–diffusive equations reduces, and sometimes removes, the need of stabilization, still providing a very accurate localization of thin internal and boundary layers.

The paper is organized as follows. After recalling advection–diffusion problems and classical stabilization techniques for finite elements setting in Section 2, the isogeometric analysis approach based on generalized B-splines is briefly reviewed in Section 3, focussing on exponential and variable degree splines. Section 4 illustrates the performances of IgA based on exponential and variable degree B-splines in the context of advection–diffusion problems by means of some computed examples. Section 5 makes some concluding remarks.

2. Advection–diffusion equation and stabilization methods

Let $\Omega \subset \mathbb{R}^d$ be an open bounded region with piecewise smooth boundary $\partial\Omega$, with $d = 2, 3$. The advection–diffusion equation is given by

$$-\nabla \cdot (\kappa \nabla u) + \mathbf{a} \cdot \nabla u = f, \quad \text{in } \Omega \tag{1}$$

where u is the unknown scalar field, $\mathbf{a}$ is the given flow velocity which is assumed solenoidal, i.e., $\nabla \cdot \mathbf{a} = 0$ in Ω, $\kappa(\mathbf{x}) > \kappa_0 > 0$ is a bounded positive function representing diffusivity, and f is the prescribed source function. For simplicity, we consider $u = 0$ on $\partial\Omega$. The generalization to non homogeneous Dirichlet conditions and/or Neumann conditions is standard, see i.e., [10,11].

The weak form of this problem is to find $u \in H_0^1(\Omega)$ such that

$$a(u, v) = F(v), \quad \forall v \in V = H_0^1(\Omega),$$

where

$$a(u, v) = \int_\Omega \kappa \nabla u \cdot \nabla v \, d\mathbf{x} + \int_\Omega v\mathbf{a} \cdot \nabla u \, d\mathbf{x}, \quad \text{and} \quad F(v) = \int_\Omega f v \, d\mathbf{x}.$$

We recall that, by the Lax–Milgram theorem, the existence of a unique solution is attained provided that the bilinear form $a(u, v)$ is coercive and continuous and the linear functional F is bounded. In particular the coercivity, $a(v, v) \geq \alpha \|v\|^2_{H^1(\Omega)}$, is obtained taking

$$\alpha = \kappa_0/(1 + C_P^2), \tag{2}$$

where C_P comes from the Poincaré inequality, [11]. Setting

$$M = \|\kappa\|_{L^\infty(\Omega)} + \|\mathbf{a}\|_{L^\infty(\Omega)}, \tag{3}$$

we have the following a priori estimates, [11]:

$$\|u\|_V \leq \frac{1}{\alpha}\|f\|_{L^2(\Omega)}, \qquad \|\nabla u\|_{L^2(\Omega)} \leq \frac{C_P}{\kappa_0}\|f\|_{L^2(\Omega)}. \tag{4}$$

Now the standard Galerkin method is obtained by substituting the space of test functions and trial solutions V, with a finite dimensional one, V_h, for instance the space of piecewise linear finite elements. The approximate solution u_h satisfies (4) and therefore it can be characterized by large gradients whenever κ_0 is small. Moreover, from the Céa Lemma we have

$$\|u - u_h\|_V \leq \frac{M}{\alpha} \inf_{w_h \in V_h} \|u - w_h\|_V.$$

From the above relation we notice in particular that the Galerkin method can have a poor performance if the coerciveness constant α is small in comparison with the continuity constant M and, recalling (2) and (3), this is the case when the ellipticity constant κ_0 is small with respect to $\|\mathbf{a}\|_{L^\infty(\Omega)}$, i.e. when the advective term dominates on the diffusive one. In particular, dealing with classical FEM, a way to measure this quantity is given by the so called Péclet number:

$$\mathbf{Pe} = \frac{\|\mathbf{a}\|h}{2\kappa_0}$$

with h the maximum of the diameters of the elements. When $\mathbf{Pe} \gg 1$ we can have a lack of stability which gives rise to wildly oscillating solutions in the presence of sharp layers. In order to overcome this issue, stabilized methods such as the SUPG and GLS methods have been developed, [1,5].

Let us recall briefly the main ideas behind stabilization methods. In order to better understand where the instabilities come from let us first consider a simple one dimensional example.

$$\begin{cases} -\kappa u'' + au' = 0, & 0 < x < 1 \\ u(0) = 0, & u(1) = 1, \end{cases} \tag{5}$$

with $0 < \kappa \ll 1$ and $a > 0$. The exact solution

$$u(x) = \frac{e^{\frac{a}{\kappa}x} - 1}{e^{\frac{a}{\kappa}} - 1}$$

exhibits a boundary layer of width $\mathcal{O}(\kappa/a)$ with gradient like a/κ near to $x = 1$ if a/κ is small enough. The Galerkin method with piecewise-linear finite elements over a uniform grid $x_j = jh,\ h = 1/n,\ j = 0, 1, \ldots, n$, produces approximations u_h of the form

$$u_h(x_j) = \frac{\left(\frac{1+\mathbf{Pe}}{1-\mathbf{Pe}}\right)^j - 1}{\left(\frac{1+\mathbf{Pe}}{1-\mathbf{Pe}}\right)^n - 1}, \quad j = 1, \ldots, n-1$$

where the *Péclet number* is now given by $\mathbf{Pe} = ah/2\kappa$.

If $\mathbf{Pe} > 1$ then $(1 + \mathbf{Pe})/(1 - \mathbf{Pe}) < 0$, and consequently the solution u_h exhibits an oscillatory behavior. Clearly, κ and a being fixed, in order to avoid oscillations, in principle it is always possible to choose the grid-size h small enough so that $\mathbf{Pe} \leq 1$. However, this is very often impractical if κ is very small with respect to a, since one would obtain huge linear systems (and actually it may be unfeasible in the higher dimensional case).

On the other hand it can be noted that the same discrete solution can be obtained by approximating (5) by *centered finite differences* and therefore the Galerkin method with piecewise-linear polynomials is equivalent to the approximation by means of centered finite differences. By observing now that in problem (5) transport occurs from left to right (as the advective coefficient a is positive), one is led to consider backward (upwind) finite differences to approximate $au'(x)$. In this way we obtain a less accurate method (the truncation error is only $\mathcal{O}(h)$), but stable for every value of h. The idea behind the stabilization methods (e.g. Upwind scheme), see for instance [11], is to introduce a numerical dissipation, called *numerical diffusion* (or *numerical viscosity*) in the equation, so that it can be regarded as considering backward (*upwind*) finite differences to approximate the term au' in (5). Indeed instead of considering (5), we may consider a *perturbed* problem with viscosity given by $\kappa_h = \kappa(1 + \mathbf{Pe})$. The new Péclet number associated with this scheme is

$$\mathbf{Pe}^* = \frac{ah}{2\kappa_h} = \frac{\mathbf{Pe}}{1 + \mathbf{Pe}} < 1.$$

Therefore we have that the Upwind method does not exhibit oscillations i.e. it is stable, for any value of h. More general methods introduce in the problem a viscosity of the form $\kappa_h = \kappa(1 + \phi(\mathbf{Pe}))$, where the function $\phi(\mathbf{Pe})$ is selected in order to increase the accuracy of the solution. As an example the Scharfetter–Gummel scheme (ϕ is an exponential function) provides a second order convergence with respect to h (optimal upwind viscosity).

Analogously to the one dimensional case, also in the two dimensional case the stabilization techniques rely on introducing a "numerical viscosity" in the streamline direction that has indeed the effect of stabilizing the computational algorithm. This can be seen as a method to solve the generalized Galerkin problem: find $u_h \in V_h$ such that

$$a_h(u_h, v_h) = F_h(v_h), \quad \forall v_h \in V_h$$

where

$$a_h(u_h, v_h) = a(u_h, v_h) + b_h(u_h, v_h), \qquad F_h(v_h) = F(v_h),$$

and b_h is a suitable bilinear form to be defined. The aim of such stabilization techniques is also that of not reducing the accuracy of the polynomial approximation inherent to the choice of the finite dimensional subspace, and this is achieved by imposing the *strong consistency* of the method, that is

$$a_h(u, v_h) - F_h(v_h) = 0, \quad \forall v_h \in V_h.$$

Now, any elliptic operator can be split into a symmetric and a skew-symmetric part:

$$L = L_S + L_{SS}.$$

For advection–diffusion equation we have

$$L_S u = -\kappa \Delta u + \left[\frac{1}{2}\mathrm{div}(\mathbf{a})\right] u, \qquad L_{SS} u = \frac{1}{2}\left[\mathrm{div}(\mathbf{a}u) + \mathbf{a} \cdot \nabla u\right].$$

A stabilized strongly consistent method can be obtained by considering the problem: find $u_h \in V_h$ such that

$$a(u_h, v_h) + \mathcal{L}_h(u_h, f, v_h) = F(v_h), \quad \forall v_h \in V_h,$$

with $\mathcal{L}_h(u, f, v_h) = 0,\ \forall v_h \in V_h$. We note that $\mathcal{L}_h$ depends on both u_h and f. A possible choice could be

$$\mathcal{L}_h^{(\rho)}(u_h, f, v_h) = \sum_{T_k \in \mathcal{T}_h} \delta(Lu_h - f, \mathcal{S}_{T_k}^{(\rho)}(v_h))_{L^2(T_k)}$$

where ρ and δ are free parameters to be fixed, T_k is a generic element of a partition, $\mathcal{T}_h$, of Ω_h which approximates the physical domain Ω, and

$$\mathcal{S}_{T_k}^{(\rho)}(v_h) = \frac{h_{T_k}}{\|\mathbf{a}\|}[L_{SS} v_h + \rho L_S v_h],$$

with h_{T_k} the diameter of T_k. Different choices of the parameter ρ lead to different methods. The most used ones are

- $\rho = 1$: Galerkin Least-Squares (GLS);
- $\rho = 0$: Streamline Upwind Petrov–Galerkin (SUPG);
- $\rho = -1$: Douglas–Wang (DW).

For every method, the choice of δ (called the stabilization parameter) is also crucial as it measures the amount of artificial viscosity, see [11] for details.

3. Isogeometric analysis based on exponential and variable degree B-splines

As mentioned in the previous section, the Galerkin approximation consists in looking for the solution in a suitable finite dimensional subspace $V_h \subset V$

$$V_h = \langle \phi_1, \phi_2, \ldots, \phi_{n_h} \rangle \subset V. \tag{6}$$

Different methods correspond to different choices of the subspace V_h.

In standard FEM the physical domain Ω is usually approximated by a polygon Ω_h which is partitioned into a mesh of elements T_k that are sub-domains of the same shape as the parameter domain Ω_0, for instance in $\mathbb{R}^2$ the reference triangle $\{(x, y) \in \mathbb{R}^2 : 0 \le x, y, x + y \le 1\}$. Each element T_k is obtained from Ω_0 by a suitable *local* invertible geometric transformation G_k. Similarly, the basis functions in (6) are compositions of a set of shape functions (usually low degree polynomials) with the inverse of the various G_k. The result is a piecewise polynomial space with C^0 continuity across element interfaces.

The main drawbacks of FEM are the lack of an exact geometry representation for complex engineering shapes – usually defined by polynomial curves and conic sections – as well as a solution space whose global smoothness is only C^0, even in the case of high order piecewise polynomial approximation spaces.

Isogeometric Analysis (IgA), introduced in [6], addresses both the previous drawbacks. Indeed, the distinguishing properties of IgA are:

- trying to bridge the gap between computer aided design (CAD) and finite element methods by adopting the same basis functions to construct both trial and test spaces in the discrete variational formulation of differential problems as are used to design domain geometries in CAD applications (typically B-splines or NURBS)[1];
- consider finite dimensional spaces of high order and regularity (usually obtained by standard CAGD basis functions) without increasing too much the degrees of freedom. This is beneficial in several applications, including a better capturing of thin layers.

To be more specific, in IgA, assuming for instance the reference domain $\Omega_0 = [0, 1] \times [0, 1]$ is given, the physical domain is obtained by a *global geometry function*

$$G : \Omega_0 \to \overline{\Omega}, \qquad G(\boldsymbol{\omega}) = \sum_{i=1}^{n_h} \mathcal{N}_i(\boldsymbol{\omega}) \mathbf{P}_i, \quad \mathbf{P}_i \in \mathbb{R}^2,\ \boldsymbol{\omega} \in \Omega_0;$$

where the basis functions $\{\mathcal{N}_1, \ldots, \mathcal{N}_{n_h}\}$, have to be selected to satisfy our requirements, for instance being able to describe sharp variations. The space V_h is then spanned by the functions

$$\phi_i(\mathbf{x}) = \mathcal{N}_i \circ G^{-1}(\mathbf{x}) = \mathcal{N}_i(\boldsymbol{\omega}), \quad i = 1, \ldots, n_h,\ \mathbf{x} = G(\boldsymbol{\omega}). \tag{7}$$

In IgA based on NURBS, basis functions are in fact NURBS but, according to [6], *NURBS are not a requisite ingredient in isogeometric analysis* and other possible bases can be suitably employed in a "problem-dependent" analysis.

As an example, generalized B-splines can be seen as a valid, and in some cases more flexible, alternative to the rational model in IgA, see [10,12]. Generalized B-splines possess all the fundamental properties of algebraic B-splines (partition of

[1] The term "isogeometric" comes from the fact that an *isoparametric* approach is considered, i.e. the solution space for dependent variables is represented in terms of the same functions which describe the geometry, where, in addition, the geometry is exactly represented and preserved since the coarsest refinement level.

unity, minimum support, local linear independence, knot insertion, ...) which are shared by NURBS as well. While classical B-splines are piecewise functions with sections in the space of algebraic polynomials, generalized B-splines are piecewise functions with sections in more general spaces. The selection of section spaces depends on the features we are interested in. If the exact description of the geometry is the main issue, generalized B-splines based on trigonometric or exponential functions can be profitably used since they allow exact representation of polynomial curves, conic sections, helices and other profiles of salient interest in applications, without the geometrical and analytical drawbacks of NURBS, see [10,12].

In this paper we are interested in the treatment of advection–diffusion problems characterized by sharp layers involving strong gradients. On this concern IgA based on B-splines with high order and high regularity leads to remarkable results, [6]. To strengthen this interesting performance, we will consider an IgA approach based on generalized spline spaces particularly well suited to describe sharp variation, still retaining a high order and smoothness. Thus we will focus on exponential and variable degree splines, whose definition and main properties will be recalled in the next subsection.

3.1. Exponential and variable degree B-splines

Assuming a sequence of knots is given

$$\Xi = \{\xi_1 \le \xi_2 \le \cdots \le \xi_{n+p}\}, \quad n, p \in \mathbb{N}, \tag{8}$$

classical B-splines of order p are piecewise polynomial functions with a suitable smoothness, i.e. functions with sections in the space of algebraic polynomials of order p

$$\mathbb{P}_p = \langle 1, t, \ldots, t^{p-3}, t^{p-2}, t^{p-1}\rangle.$$

Generalized B-splines of order p are functions with a given smoothness, see [13,14] and references therein, belonging piecewise to

$$\mathbb{P}_p^{u_i,v_i} = \langle 1, t, \ldots, t^{p-3}, u_i(t), v_i(t)\rangle, \quad t \in [\xi_i, \xi_{i+1}),\ i = 1, \ldots, n+p-1, \tag{9}$$

where u_i, v_i, are smooth functions to be selected to obtain specific features. In order to be able to describe sharp variations, suitable choices for spaces (9) are

$$\mathbb{E}_{p,\alpha_i} = \langle 1, t, \ldots, t^{p-3}, \mathrm{e}^{\alpha_i t}, \mathrm{e}^{-\alpha_i t}\rangle, \quad 0 < \alpha_i \in \mathbb{R}, \tag{10}$$

$$\mathbb{VD}_{p,\lambda_i} = \langle 1, \tau, \ldots, \tau^{p-3}, (1-\tau)^{\lambda_i}, \tau^{\lambda_i}\rangle, \quad p-1 \le \lambda_i \in \mathbb{R}, \tag{11}$$

for the local parameter τ such that $\tau = (t-\xi_i)/h_i$ and $h_i = \xi_{i+1} - \xi_i$.

It is well known that it is possible to construct B-spline like functions with sections in spaces (10) and (11), see [15–20] and the references therein.[2] We will refer to these splines as exponential and variable degree splines of order p respectively and we will denote them by $N_{i,\Xi}^{(p)},\ i = 1, \ldots, n$.[3]

Exponential and variable degree B-splines possess all desirable properties of classical polynomial B-splines, [22,15,18]. For notational convenience we state the following.

Proposition 1. *Let $N_{i,\Xi}^{(p)},\ i = 1, \ldots, n$, denote the exponential or variable degree B-splines of order p associated to the sequence of knots (8). Then the following properties hold.*

- *positivity:* $N_{i,\Xi}^{(p)}(t) \ge 0$,
- *partition of unity:* $\sum_{i=1}^{n} N_{i,\Xi}^{(p)}(t) \equiv 1,\ t \in [\xi_p, \xi_{n+1}]$,
- *compact support:* $N_{i,\Xi}^{(p)}(t) = 0,\ t \notin [\xi_i, \xi_{i+p}]$,
- *smoothness:* $N_{i,\Xi}^{(p)}(t)$ *is* $p - \rho_j - 1$ *times continuously differentiable at* ξ_j *being* ρ_j *the multiplicity of* ξ_j *in the knot sequence,*
- *local linear independence:* $N_{i-p+1,\Xi}^{(p)}(t), \ldots, N_{i-1,\Xi}^{(p)}(t), N_{i,\Xi}^{(p)}(t)$ *are linearly independent on* $[\xi_i, \xi_{i+1}]$.

In addition, exponential and variable degree B-splines support a knot insertion procedure, [15,20], as well as a degree-raising process. Thus, refinement processes of common use in isogeometric analysis based on NURBS (h, p, and k-refinement, [6]) can be extended to isogeometric analysis based on exponential and variable degree B-splines.

For a given order p and a fixed sequence of knots Ξ, we will denote by

$$\mathbb{S}_{\Xi}^{p}, \qquad \mathbb{ES}_{\Xi,\boldsymbol{\alpha}}^{p}, \qquad \mathbb{VDS}_{\Xi,\boldsymbol{\lambda}}^{p}$$

the spaces spanned by classical B-splines, exponential B-splines, variable degree B-splines respectively, where $\boldsymbol{\alpha} = \{\ldots, \alpha_i, \ldots\}$, $\boldsymbol{\lambda} = \{\ldots, \lambda_i, \ldots\}$ denote the sets of real parameters as in (10) and (11). We will refer to $\mathbb{ES}_{\Xi,\boldsymbol{\alpha}}^{p}$, $\mathbb{VDS}_{\Xi,\boldsymbol{\lambda}}^{p}$ as *exponential splines* and *variable degree splines* respectively.

---

[2] For the approximation power of spaces (10) and (11) see [15,13,21,14].

[3] To simplify the notation we use the same symbol both for exponential and variable degree B-splines. The specific section space will be clear from the context.

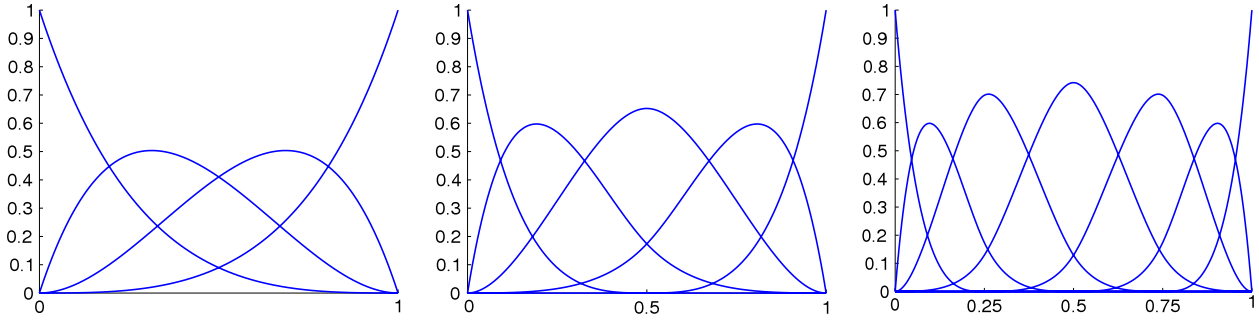

Fig. 1. Exponential B-splines of order 4 with $\alpha_i = 3h$ and knot sequence $\Xi = \{0,\ 0,\ 0,\ 0,\ h,\ 2h, \ldots,\ 1,\ 1,\ 1,\ 1\},\ h = 1/n,\ n = 1, 2, 4$.

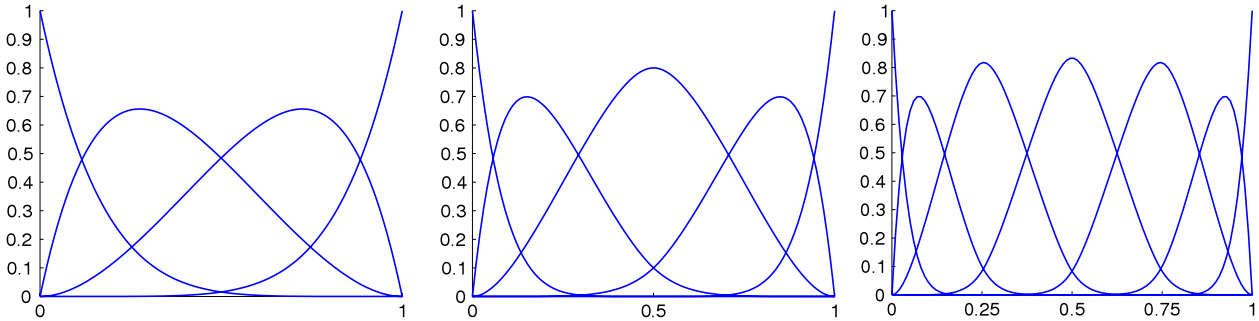

Fig. 2. Variable degree B-splines of order 4 with $\lambda_i = 6$ and knot sequence $\Xi = \{0,\ 0,\ 0,\ 0,\ h,\ 2h, \ldots,\ 1,\ 1,\ 1,\ 1\},\ h = 1/n,\ n = 1, 2, 4$.

Exponential splines of order 4 were introduced in [23] to face the problem of shape-preserving interpolation. The parameters $\boldsymbol{\alpha}$ act as *shape parameters* for $\mathbb{ES}^p_{\Xi,\boldsymbol{\alpha}}$. The space approaches $\mathbb{S}^p_\Xi$ as α_i tends to 0 (see Figs. 1 and 3). On the other hand, as α_i tends to ∞ we have a tension effect. In particular the space $\mathbb{ES}^4_{\Xi,\boldsymbol{\alpha}}$ approaches the space of linear splines (see Fig. 3).

The computational difficulties related to the evaluation of exponential functions motivated the introduction of different function spaces to address the problem of shape-preserving interpolation and approximation. Among the others, variable degree polynomial splines were successfully introduced some years ago, [15], as a valid alternative to exponential splines and used in several applications ranging from functional one-dimensional interpolation, to scattered data interpolation, to 3D interpolation or approximation of parametric curves, see [16,24] and the references therein.

Variable degree splines possess tension properties analogous to exponential splines as the parameters λ_i increase, see Figs. 2, 4.

Their main feature is in their geometric simplicity, and in their efficient evaluation. Indeed, it can be shown that such splines can be obtained by a *geometric construction* consisting in simple corner cutting schemes which are applied to the (generalized) de Boor control polygon and produce the (generalized) Bézier control polygons associated with the Bernstein like representation of the section spaces (11), [15,25]. Thanks to this geometric construction, the evaluation of the spline results in a stable computation.

Such geometric construction can be extended to splines with section spaces of the form:

$$\mathbb{VDQ}_{6,\lambda_i} = \langle 1, \tau, (1-\tau)^{\lambda_i}, \tau(1-\tau)^{\lambda_i-1}, (1-\tau)\tau^{\lambda_i-1}, \tau^{\lambda_i}\rangle, \quad 5 \le \lambda_i, \tag{12}$$

where $\tau = (t - \xi_i)/h_i$. These spaces were introduced in [16] and have tension properties similar to spaces $\mathbb{VD}_{4,\lambda_i}$. As for spaces (10) and (11), it is possible to construct B-spline like functions with sections in spaces of the form (12), see Fig. 5. In particular, C^3 spline functions with sections in (12) possess a nice geometric construction and easy to handle shape-preserving properties. We will denote them by $\mathbb{VDQS}^6_{\Xi,\boldsymbol{\lambda}}$. The reader is referred to [16,26] for a more detailed description of these spaces and of the geometric construction of the related B-spline like basis[4,5].

Summarizing, thanks to their ability to describe sharp variations and to the possibility of easily managing high smoothness, the B-spline like functions belonging to spaces $\mathbb{ES}^p_{\Xi,\boldsymbol{\alpha}}$, $\mathbb{VDS}^p_{\Xi,\boldsymbol{\lambda}}$ and $\mathbb{VDQS}^6_{\Xi,\boldsymbol{\lambda}}$ are good candidates to replace standard B-splines (and NURBS) in isogeometric analysis for advection–diffusion problems.

Exponential splines are particularly attractive because, for suitable selections of $\boldsymbol{\alpha}$, they are the fundamental solutions of (1) in the one dimensional case for constant coefficients, see Example 1 in Section 4. Nevertheless, dealing with spaces $\mathbb{ES}^p_{\Xi,\boldsymbol{\alpha}}$, incurs computational difficulties for evaluation of the basis elements and their derivatives, mainly for large values

[4] So far the complete B-spline theory for spaces (12) has been developed only for integer exponents.

[5] For the sake of simplicity we will denote by $N^{(p)}_{i,\Xi}$ also the B-spline like basis elements in $\mathbb{VDQS}^6_{\Xi,\boldsymbol{\lambda}}$.

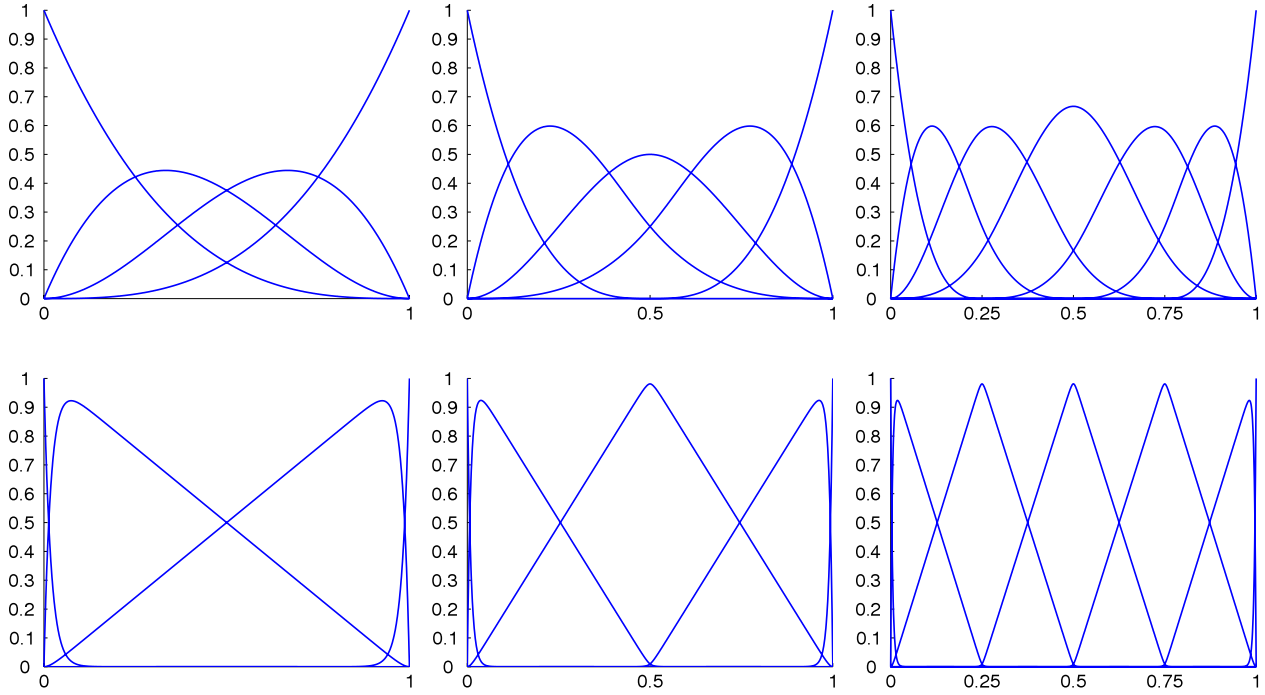

Fig. 3. Exponential B-splines of order 4 with $\alpha_i = 0.1h$ (top), $\alpha_i = 50$ (down), and knot sequence $\Xi = \{0,\ 0,\ 0,\ 0,\ h,\ 2h, \ldots,\ 1,\ 1,\ 1,\ 1\}$, $h = 1/n$, $n = 1, 2, 4$.

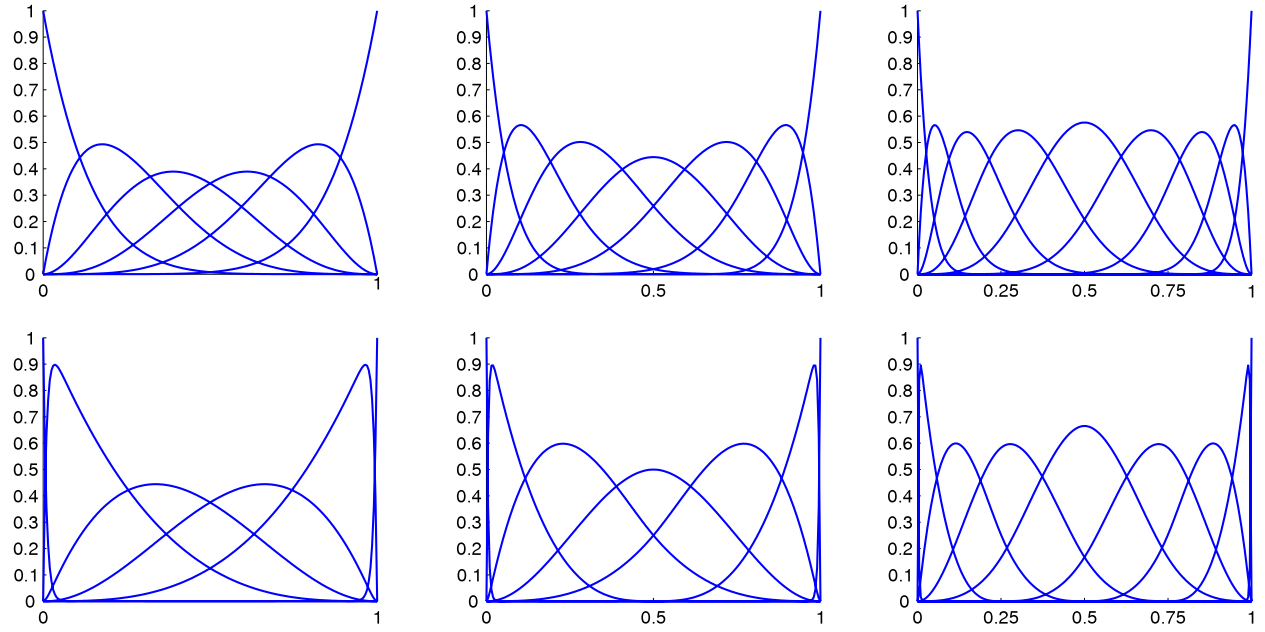

Fig. 4. Variable degree B-splines of order 6 with $\lambda_i = 6$ (top), $\lambda_i = 100$ (down), and knot sequence $\Xi = \{0,\ 0,\ 0,\ 0,\ h,\ 2h, \ldots,\ 1,\ 1,\ 1,\ 1\}$, $h = 1/n$, $n = 1, 2, 4$.

of the parameters $\boldsymbol{\alpha}$.[6] On the other hand, $\mathbb{VDS}^p_{\Xi,\boldsymbol{\lambda}}$ and $\mathbb{VDQS}^6_{\Xi,\boldsymbol{\lambda}}$ with integer exponents have a special appeal thanks to the geometric construction and low computational cost of the related B-spline bases. In particular it can be proved, [15,16], that the computational cost for the evaluation of elements in $\mathbb{VDS}^p_{\Xi,\boldsymbol{\lambda}}$ and $\mathbb{VDQS}^6_{\Xi,\boldsymbol{\lambda}}$ is comparable with the cost of evaluation of classical cubic and quintic splines respectively. Therefore variable degree splines are preferable in practical applications.

To take into account these two aspects we prefer to consider $\mathbb{VDS}^p_{\Xi,\boldsymbol{\lambda}}$ and $\mathbb{VDQS}^6_{\Xi,\boldsymbol{\lambda}}$ as approximating spaces, selecting the exponents so that such spaces mimic a given space $\mathbb{ES}^p_{\Xi,\boldsymbol{\alpha}}$. Some strategies for selecting exponents will be described in the next subsection.

[6] Nonstationary subdivision algorithms seem to be the most promising evaluation strategy for evaluating the elements of $\mathbb{ES}^p_{\Xi,\boldsymbol{\alpha}}$, [27].

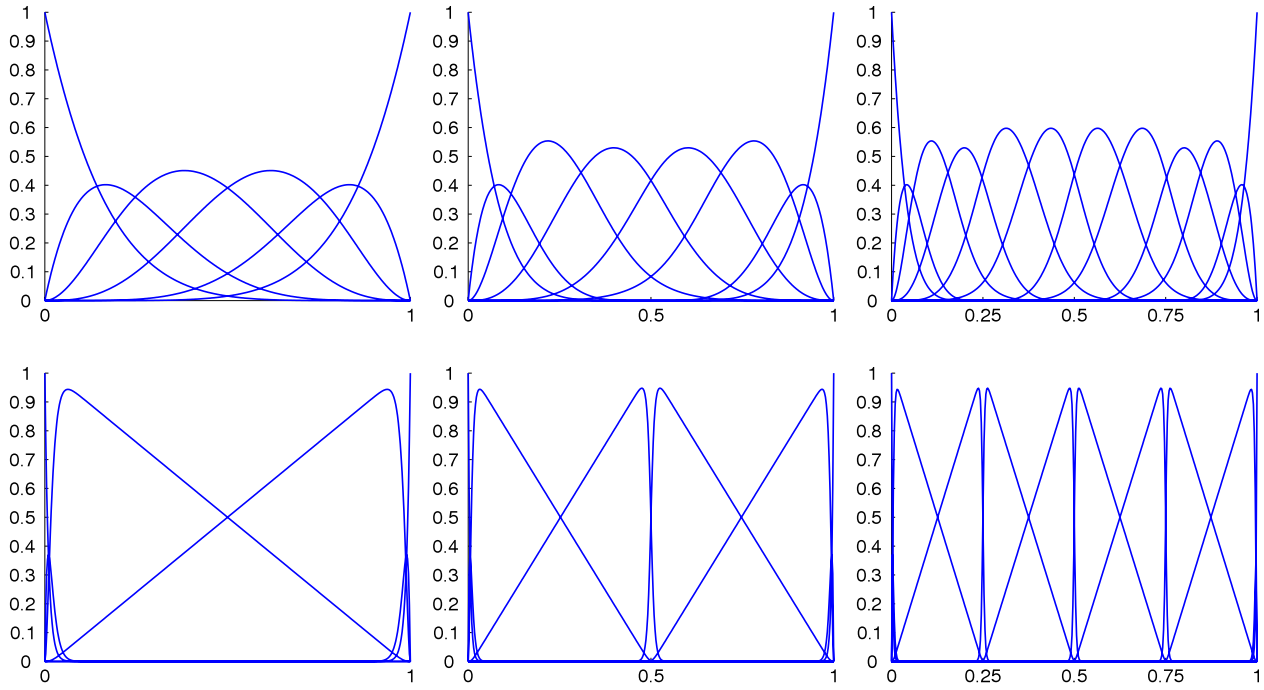

Fig. 5. B-splines in $\mathbb{VDQS}^6_{\Xi,\boldsymbol{\lambda}}$ with $\lambda_i = 6$ (top), $\lambda_i = 100$ (down) and $\Xi = \{0,\ 0,\ 0,\ 0,\ h,\ h,\ 2h,\ 2h, \ldots,\ 1,\ 1,\ 1,\ 1\}$, $h = 1/n$, $n = 1, 2, 4$.

3.2. Selection of tension parameters in $\mathbb{VDS}^4_{\Xi,\boldsymbol{\lambda}}$

We present some very simple strategies that can be used for the automatic selection of the degree parameters in $\mathbb{VDS}^4_{\Xi,\boldsymbol{\lambda}}$, in order to reproduce the behavior of exponential splines in $\mathbb{ES}^4_{\Xi,\boldsymbol{\alpha}}$ for fixed $\boldsymbol{\alpha}$.

On a generic interval $[\xi_i, \xi_{i+1}]$ the section spaces (10) and (11) of the spline spaces $\mathbb{VDS}^4_{\Xi,\boldsymbol{\lambda}}$ and $\mathbb{ES}^4_{\Xi,\boldsymbol{\alpha}}$ are respectively

$$\langle 1, \tau, (1-\tau)^{\lambda_i}, \tau^{\lambda_i}\rangle, \qquad h_i = \xi_{i+1} - \xi_i, \quad \tau = (t-\xi_i)/h_i \tag{13}$$

$$\langle 1, \tau, \mathrm{e}^{-\nu_i\tau}, \mathrm{e}^{\nu_i\tau}\rangle, \quad \nu_i = h_i\alpha_i,\ h_i = \xi_{i+1} - \xi_i,\ \tau = (t-\xi_i)/h_i. \tag{14}$$

According to [13], spaces (13) and (14) possess a unique Bernstein like basis, that is a basis $\{B_0,\ B_1,\ B_2,\ B_3\}$ such that $\sum_{i=0}^3 B_i(t) \equiv 1$ and

$$B_0(0) = B_3(1) = 1, \qquad B_0^{(k)}(1) = B_3^{(k)}(0) = 0, \quad k = 0, 1, 2,$$
$$B_1(0) = B_2(1) = 0, \qquad B_1^{(k)}(1) = B_2^{(k)}(0) = 0, \quad k = 0, 1.$$

Let ν_i be given, then we select λ_i so that the Bernstein like basis of (13) mimics the corresponding basis of (14). Although more refined and involved procedures could be addressed, we consider the following ones which are simultaneously simple and effective. Noting that τ^{λ_i} is the last element of the Bernstein like basis for (13), denoting by B_{3,ν_i} the corresponding element of the Bernstein like basis for (14), it is easy to see that

$$B_{3,\nu_i}(\tau) = \frac{2\nu_i\tau + \mathrm{e}^{-\nu_i\tau} - \mathrm{e}^{\nu_i\tau}}{2\nu_i - \mathrm{e}^{\nu_i} + \mathrm{e}^{-\nu_i}}.$$

Then, we propose two possible strategies based on the integral and on the derivative of B_{3,ν_i} respectively.

- Determine λ_i so that $\int_0^1 (\tau^{\lambda_i} - B_{3,\nu_i}(\tau))\,\mathrm{d}\tau = 0$, thus we obtain

$$\lambda_i = F_{4,\mathbf{i}}(\nu_i), \quad F_{4,\mathbf{i}}(\nu) = \frac{\mathrm{e}^{2\nu}(1-\nu) + \mathrm{e}^{\nu}(\nu^2-2) + \nu + 1}{\mathrm{e}^{\nu}(\nu^2+2) - \mathrm{e}^{2\nu} - 1}. \tag{15}$$

- Determine λ_i such that $D(\tau^{\lambda_i})|_{\tau=1} = D(B_{3,\nu_i}(\tau))|_{\tau=1}$ thus we obtain

$$\lambda_i = F_{4,\mathbf{d}}(\nu_i), \quad F_{4,\mathbf{d}}(\nu) = \frac{\nu(2 - \mathrm{e}^{\nu} - \mathrm{e}^{-\nu})}{2\nu - \mathrm{e}^{\nu} + \mathrm{e}^{-\nu}}. \tag{16}$$

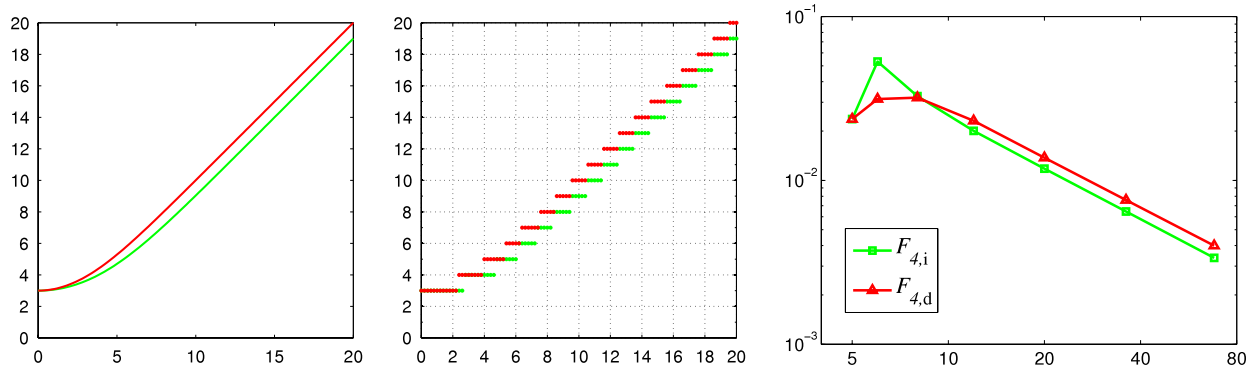

Fig. 6. Left: graph of functions $F_{4,\mathbf{i}}$ (green) and $F_{4,\mathbf{d}}$ (red). Center: their rounded counterpart. Right: graph of the error $\|\tau^{\lambda} - B_{3,\alpha}(\tau)\|_{L^\infty}$ for $\lambda = F_{4,\mathbf{i}}(\alpha)$ (green) and $\lambda = F_{4,\mathbf{d}}(\alpha)$ (red) (For interpretation of the references to colour in this figure legend, the reader is referred to the web version of this article.)

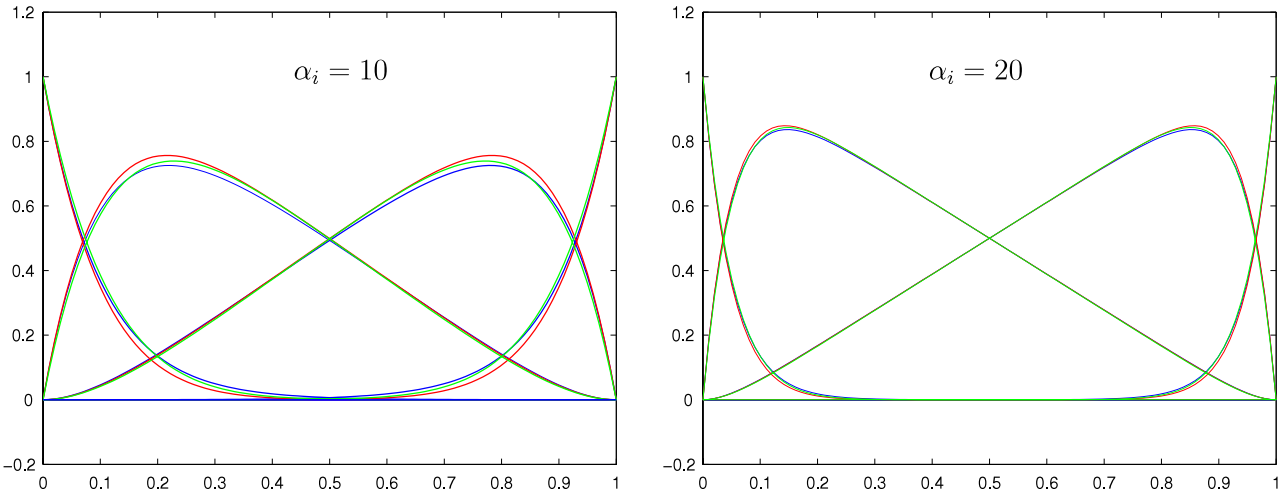

Fig. 7. Bernstein like basis in $[\xi_i, \xi_{i+1}] = [0, 1]$ for spaces (14) (blue), and (13) with $\lambda_i = F_{4,\mathbf{i}}(h_i\alpha_i)$ (green) and $\lambda_i = F_{4,\mathbf{d}}(h_i\alpha_i)$ (red), $h_i = 1$ for different α_i (For interpretation of the references to colour in this figure legend, the reader is referred to the web version of this article.)

Generally, expressions (15) and (16) do not provide integer values, thus, in order to keep low the computational cost and deal with polynomial approximating spaces, we consider the corresponding rounded values. Fig. 6 (left) shows the graphs of $F_{4,\mathbf{i}}(\nu)$, $F_{4,\mathbf{d}}(\nu)$. Note that both functions tend to 3 as ν tends to 0 according to the well known behavior of exponential splines. The rounded counterparts are depicted in Fig. 6 (center). In Fig. 7 the Bernstein like basis for the restriction to a single interval of $\mathbb{ES}^4_{\Xi,\boldsymbol{\alpha}}$ is compared to those of $\mathbb{VDS}^4_{\Xi,\boldsymbol{\lambda}}$, where the degrees are selected according to the two different functions $F_{4,\mathbf{i}}(\nu)$ and $F_{4,\mathbf{d}}(\nu)$. The errors $\|\tau^{\lambda_i} - B_{3,\nu_i}(\tau)\|_{L^\infty}$ are reported in Fig. 6 (left) for different α_i and $h_i = 1$.

The selection of parameters for $\mathbb{VDQS}^6_{\Xi,\tilde{\boldsymbol{\lambda}}}$ can be done following a completely similar strategy. We omit the details.

4. Numerical examples

In this section we present the performances of IgA based on exponential and variable degree splines for advection–diffusion (AD) problems. Since the tension parameters can be suitably selected to avoid extraneous oscillations, such an approach reduces the need of stabilization procedures which produce stable but less accurate solutions, see Section 2.

Our method can be considered as a "problem dependent" procedure since the approximation space is (automatically) properly selected depending on the specific problem we deal with. Such an approach has been previously addressed in the literature, see as an example [28] in the context of collocation.

In order to better understand the problem, first we consider a simple monodimensional example, then we present some bidimensional AD problems (1) for different setting of advection and diffusion parameters and boundary conditions.

In more detail, in the one dimensional case, the Galerkin approximation space (6) is taken as exponential or variable degree splines or $\mathbb{VDQS}^6_{\Xi,\boldsymbol{\lambda}}$ defined in Section 3.1 and the basis elements ϕ_i in (6) are the corresponding B-spline like functions $N^{(p)}_{i,\Xi}$ (see Proposition 1).

For the two dimensional examples, according to the standard paradigm of IgA based on NURBS, where functions $\mathcal{N}_i$ in (7) are tensor product NURBS, we consider tensor product exponential or variable degree B-splines (see [10] for more details).

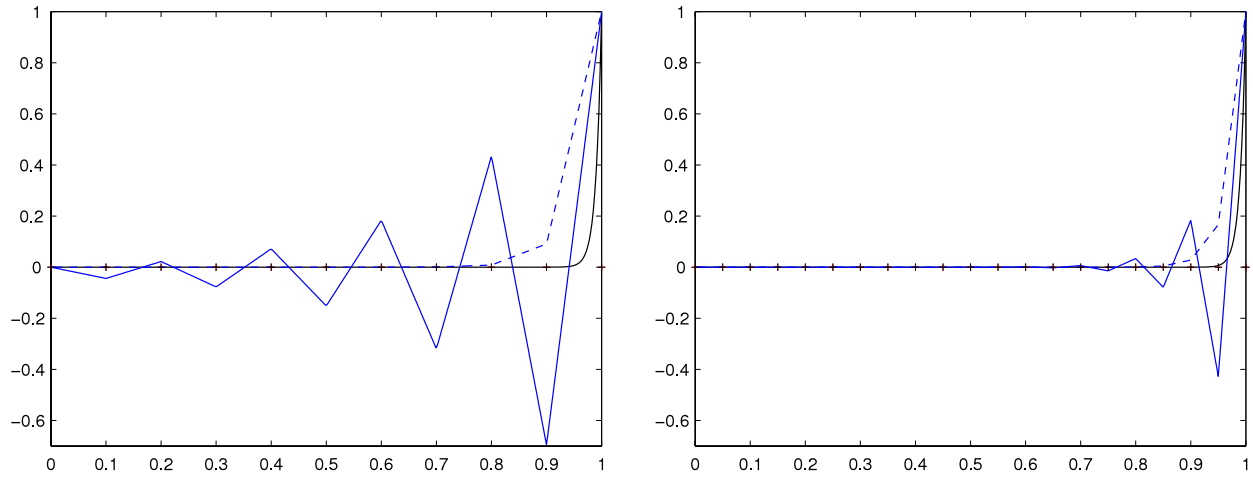

Fig. 8. Example 1. The exact solution (solid black) and the numerical approximation by using linear FEM with (dashed) and without Upwind stabilization (solid): $\mathbf{Pe} = 5,\ h = 0.1$ (left) and $\mathbf{Pe} = 2.5,\ h = 0.05$ (right).

Thus, given two sequences of knots:

$$\Xi = \{0 = \xi_1 = \cdots = \xi_p < \cdots < \xi_{n+1} = \xi_{n+p} = 1\},$$
$$\Theta = \{0 = \theta_1 = \cdots = \theta_p < \cdots < \theta_{m+1} = \theta_{m+q} = 1\},$$

we will consider the following spaces:

- $\mathbb{ES}^p_{\Xi,\boldsymbol{\alpha}} \otimes \mathbb{ES}^q_{\Theta,\boldsymbol{\beta}}$ with two sequences of strictly positive parameters:
$$\boldsymbol{\alpha} = \{\alpha_1, \alpha_2, \ldots, \alpha_{n+p-1}\}, \qquad \boldsymbol{\beta} = \{\beta_1, \beta_2, \ldots, \beta_{m+q-1}\}.$$
- $\mathbb{VDS}^p_{\Xi,\boldsymbol{\lambda}} \otimes \mathbb{VDS}^q_{\Theta,\boldsymbol{\gamma}}$ with two sequences of parameters:
$$\boldsymbol{\lambda} = \{\lambda_1, \lambda_2, \ldots, \lambda_{n+p-1}\}, \qquad \boldsymbol{\gamma} = \{\gamma_1, \gamma_2, \ldots, \gamma_{m+q-1}\}, \quad \lambda_i \geq p-1,\ \gamma_j \geq q-1.$$
- $\mathbb{VDQS}^p_{\Xi,\boldsymbol{\lambda}} \otimes \mathbb{VDQS}^q_{\Theta,\boldsymbol{\gamma}}$ with $p = q = 6$ and two sequences of parameters:
$$\boldsymbol{\lambda} = \{\lambda_1, \lambda_2, \ldots, \lambda_{n+5}\}, \qquad \boldsymbol{\gamma} = \{\gamma_1, \gamma_2, \ldots, \gamma_{m+5}\}, \quad \lambda_i, \gamma_j \geq 5.$$

Then, see Section 3, $n_h = n \cdot m$ and the functions $\mathcal{N}_i$ in (7), determining the Galerkin projection spaces (6), are the corresponding (tensor-product) B-spline like basis

$$\mathcal{N}_i = N^{(p)}_{l,\Xi} N^{(q)}_{j,\Theta}, \quad i = (j-1)n + l,\ l = 1, \ldots, n,\ j = 1, \ldots, m. \tag{17}$$

We emphasize that our approach fits in the general environment of IgA because the approximating spaces we deal with have a tensor product structure and high global smoothness as NURBS, but the treatment of the geometry is not our main issue. We recall that the distinguishing property of IgA, jointly to the (exact) description of the geometry, is to benefit from additional global smoothness.[7] Actually, despite the term "isogeometric", in the novel approach introduced in [6], dealing with approximating spaces of high smoothness seems to be as relevant as the appropriate geometry description. Thus, apart from the tutorial one dimensional example, we deliberately focus on classical examples taken from the literature for AD problems, which are challenging tests both for IgA and FEM methods. In all cases the domain is the unit square and the global geometry function, see Section 3, is the identity map.

For the same reason, in all the bivariate examples we use as approximating spaces tensor product structures based on $\mathbb{ES}^4$, $\mathbb{VDS}^4$, $\mathbb{VDQS}^6$. However, if spaces containing polynomials of higher degree, say $p-3$, are necessary then $\mathbb{ES}^p$, $\mathbb{VDS}^p$ can be considered for any p, see (10) and (11). We refer to [29] for a geometrical construction of the B-spline like basis in $\mathbb{VDS}^5$, and to [12] and reference therein for the general case.

4.1. Example 1: one dimensional AD problem

In this example we consider the one-dimensional advection–diffusion equation introduced in (5) with $\kappa = 10^{-2}$, $a = 1$. Since a/κ is small, the solution exhibits a boundary layer of width $\mathcal{O}(\kappa/a)$ near to $x = 1$ and the classical Galerkin method requires stabilization techniques.

[7] *…smoother derivatives may lead to more accurate physical quantities, such as strains and stresses, and increased smoothness may, surprisingly, lead to better capturing of thin layers,* [6].

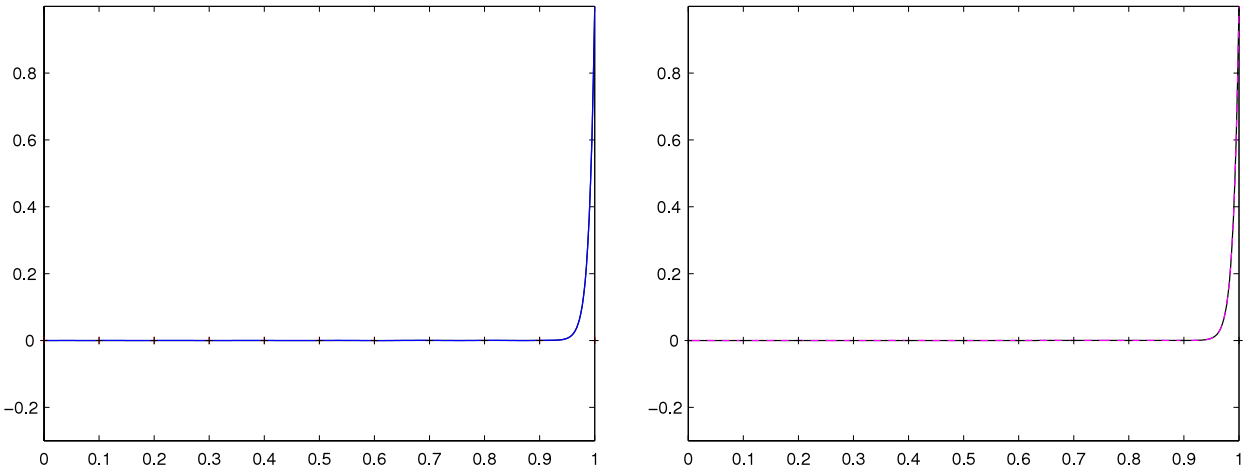

Fig. 9. Example 1. The exact solution (solid black) is compared with different numerical approximations obtained without stabilization, in $\mathbb{S}^{13}_{\Xi}$ (left) and $\mathbb{ES}^4_{\Xi,\boldsymbol{\alpha}}$ (right). **Pe** $= 5$.

Table 1
Example 1. Error in L^∞-norm versus interval number.

	UP FEM $\mathbb{P}_2$	$\mathbb{S}^4_{\Xi}$	$\mathbb{VDS}^4_{\Xi,\boldsymbol{\lambda}}$	$\mathbb{VDQS}^6_{\overline{\Xi},\bar{\boldsymbol{\lambda}}}$
2	3.1644e+00	9.0321e−01	4.0934e−03	4.0397e−03
5	8.0737e−01	4.7271e−01	7.1342e−03	7.5851e−03
10	6.9059e−01	2.4653e−01	6.7001e−03	8.7706e−03
20	5.3458e−01	6.9246e−02	1.4211e−02	4.7381e−03
40	3.5635e−01	1.2841e−02	7.1038e−03	2.5590e−04
80	1.9435e−01	1.2936e−03	1.2936e−03	1.1328e−05

In Fig. 8 we compare the exact solution and the numerical solution with linear FEM with and without Upwind stabilization, for different knot interval spacing. We can notice that the Upwind stabilization scheme produces a stable but less accurate solution. Indeed it introduces a local truncation error of order $\mathcal{O}(h)$, whereas the centered difference is of order $\mathcal{O}(h^2)$.

As an alternative we consider the numerical solution of (5) in the spaces of generalized splines of the form described in Section 3.1.

In this case the exact solution belongs to spaces of exponential splines with $p \geq 3$ for proper choice of the tension parameters. In particular, taking $\alpha_j = a/\kappa = 100,\ \forall j$, for the space $\mathbb{ES}^4_{\Xi,\boldsymbol{\alpha}}$ $(p = 4)$ defined on the knots

$$\Xi = \{0,\ 0,\ 0,\ 0,\ h,\ 2h,\ \ldots, 1,\ 1,\ 1,\ 1\}, \tag{18}$$

the solution of (5) can be exactly reproduced, as it is shown in Fig. 9 (right) for the refinement level with $h = 0.1$.

Accurate and stable results can be also obtained with classical B-spline spaces of high order without the need of stabilization techniques. An example is reported in Fig. 9 (left) for the case $p = 13$, $h = 0.1$ with an L^∞ error of the order 10^{-4}. However in this case the condition number of the system is extremely high, as it is reported in the Table 4 for all the used spaces.

In order to keep the computational cost low, we can consider the space of variable degree splines of order $p = 4$ with C^2 continuity, $\mathbb{VDS}^4_{\Xi,\boldsymbol{\lambda}}$, on the knot sequence Ξ. The parameters λ_j are selected to mimic the behavior of exponential splines in $\mathbb{ES}^4_{\Xi,\boldsymbol{\alpha}}$. More precisely, suitable values of λ_j are obtained rounding the functions $F_{4,\mathbf{i}}$ or $F_{4,\mathbf{d}}$, see (15) and (16), as described in Section 3.2. The used degrees are depicted in Table 3. We also consider the approximate solution in the space $\mathbb{VDQS}^6_{\bar{\boldsymbol{\lambda}},\overline{\Xi}}$, consisting of C^3 functions defined on the knot sequence

$$\overline{\Xi} = \{0,\ 0,\ 0,\ 0,\ 0,\ 0,\ h,\ h,\ 2h,\ 2h, \ldots,\ 1,\ 1,\ 1,\ 1,\ 1,\ 1\}. \tag{19}$$

The parameters $\bar{\lambda}_j$ will be selected according to a strategy similar to the case $\mathbb{VDS}^4_{\boldsymbol{\lambda},\Xi}$. The used degrees are depicted in Table 3 as well.

The results obtained in $\mathbb{VDS}^4_{\Xi,\boldsymbol{\lambda}}$ and $\mathbb{VDQS}^6_{\bar{\boldsymbol{\lambda}},\overline{\Xi}}$ are compared with the performance of a classical cubic spline space, $\mathbb{S}^4_{\Xi}$, and with classical linear finite element methods, FEM $\mathbb{P}_2$, with Upwind stabilization. Table 1 collects the L^∞-norm of the corresponding errors.

Without any stabilization classical cubic splines produce solutions characterized by high oscillations, see Fig. 10 (left).

Instead, the solution in $\mathbb{VDS}^4_{\Xi,\boldsymbol{\lambda}}$ presents only some small oscillations which disappear in finer meshes, meanwhile the solution in the richer space $\mathbb{VDQS}^6_{\bar{\boldsymbol{\lambda}},\overline{\Xi}}$ is stable even at coarse level, see Fig. 10 (right: center and bottom). Moreover, these

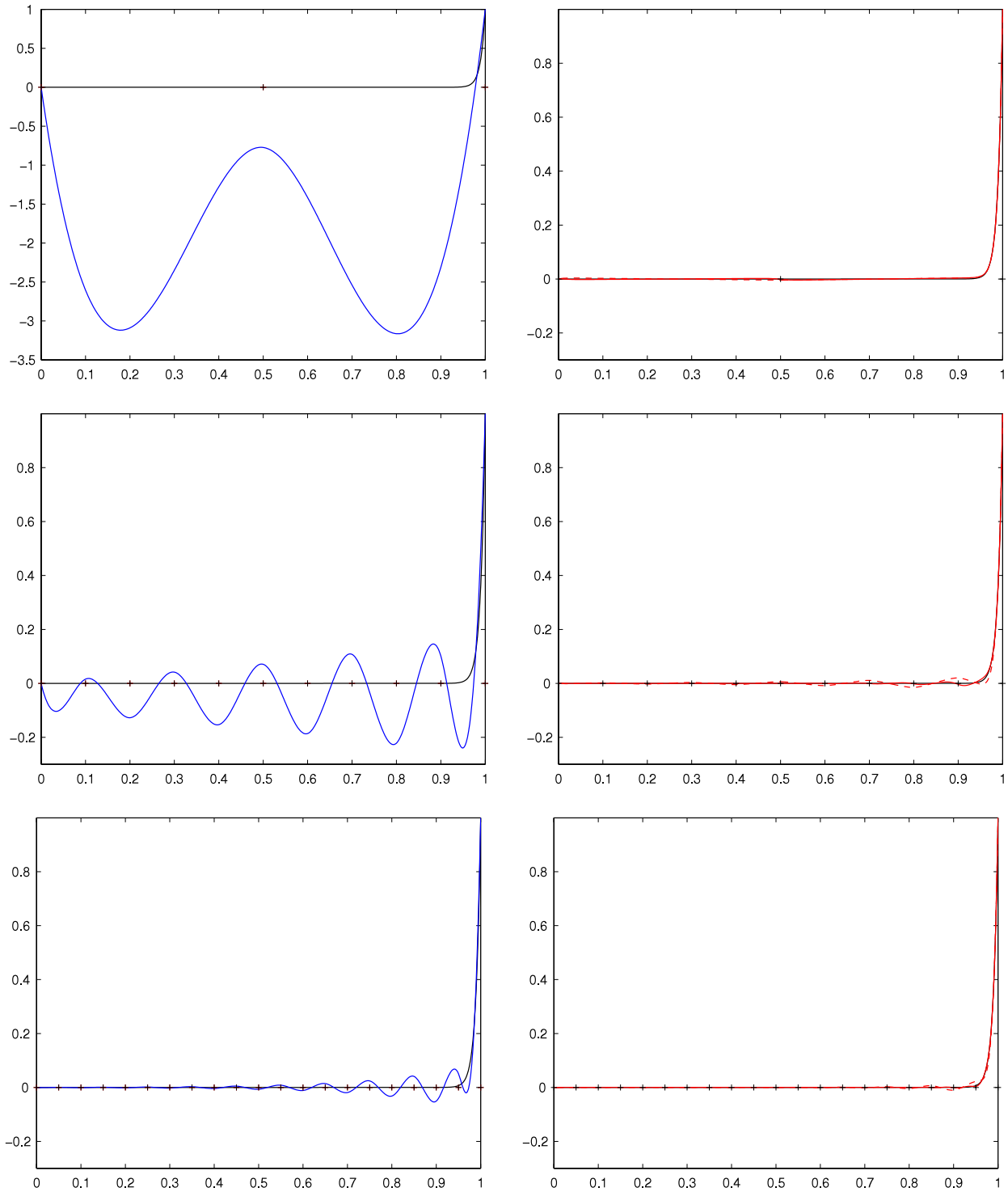

Fig. 10. Example 1. The exact solution (solid black) is compared with different numerical approximations obtained without stabilization. From top to bottom: **Pe** $= 25, 5, 2.5$ and $h = 0.5, 0.1, 0.05$. Left: $\mathbb{S}^4_{\Xi}$. Right: $\mathbb{VDS}^4_{\Xi,\boldsymbol{\lambda}}$ (dashed red) and $\mathbb{VDQS}^6_{\Xi,\boldsymbol{\lambda}}$ (solid red) (For interpretation of the references to colour in this figure legend, the reader is referred to the web version of this article.)

spaces are capable of better reproducing the behavior of exponential splines in very coarse meshes, but only by adopting high degrees. Fig. 10 (top-right) shows the results by using a 2-interval mesh. In such a case $\mathbb{VDS}^4_{\Xi,\boldsymbol{\lambda}}$ and $\mathbb{VDQS}^6_{\bar{\boldsymbol{\lambda}},\bar{\Xi}}$ mimic $\mathbb{ES}^4_{\Xi,\boldsymbol{\alpha}}$ very well (see Fig. 6 right), but require high exponents, actually $\lambda_j = \bar{\lambda}_j = 50$.

We remark that such results have been obtained without using any stabilization techniques. Table 2 collects the amount of degrees of freedom involved.

Finally we notice from Table 4, that the condition number in 2-norm of the system corresponding to spaces of generalized B-splines is extremely low and for instance considering $\mathbb{VDS}^4_{\Xi,\boldsymbol{\lambda}}$ and $\mathbb{ES}^4_{\Xi,\boldsymbol{\alpha}}$, it behaves as the condition number in $\mathbb{S}^4_{\Xi}$.

Table 2
Example 1. Degrees of freedom versus interval number.

	(UP) FEM $\mathbb{P}_2$	$\mathbb{S}^4_{\Xi}$	$\mathbb{S}^{13}_{\Xi}$	$\mathbb{ES}^4_{\Xi,\boldsymbol{\alpha}}$	$\mathbb{VDS}^4_{\Xi,\boldsymbol{\lambda}}$	$\mathbb{VDQS}^6_{\overline{\Xi},\bar{\boldsymbol{\lambda}}}$
2	3	5	17	5	5	14
5	6	8	17	8	8	14
10	11	13	22	13	13	24
20	21	23	32	23	23	44
40	41	43	52	43	43	84
80	81	83	92	83	83	164

Table 3
Example 1. Parameters $\boldsymbol{\alpha}$, $\boldsymbol{\lambda}$ and $\bar{\boldsymbol{\lambda}}$ versus interval number.

	$\mathbb{ES}^4_{\Xi,\boldsymbol{\alpha}}$	$\mathbb{VDS}^4_{\Xi,\boldsymbol{\lambda}}$	$\mathbb{VDQS}^6_{\overline{\Xi},\bar{\boldsymbol{\lambda}}}$
2	100	50	50
5	100	20	20
10	100	10	11
20	100	5	7
40	100	4	5
80	100	3	5

Table 4
Example 1. Condition number in 2-norm versus interval number.

	(UP) FEM $\mathbb{P}_2$	$\mathbb{S}^4_{\Xi}$	$\mathbb{S}^{13}_{\Xi}$	$\mathbb{ES}^4_{\Xi,\boldsymbol{\alpha}}$	$\mathbb{VDS}^4_{\Xi,\boldsymbol{\lambda}}$	$\mathbb{VDQS}^6_{\overline{\Xi},\bar{\boldsymbol{\lambda}}}$
5	5.7	5.8	3.0e+05	3.7	3.7	7.7
10	13.8	11.2	1.0e+05	6.8	6.8	12.4
20	23.5	10.6	5.1e+04	12.1	12.1	20.8
40	88.0	21.3	4.7e+04	23.1	25.4	49.0
80	256.7	67.5	4.7e+04	69.0	67.5	146.2

On the other hand, the high condition number in $\mathbb{S}^{13}_{\Xi}$, and its anomalous behavior, forebode possible numerical difficulties in dealing with such spaces.

4.2. Example 2: homogeneous problem on a square

In this example we consider the advection–diffusion equation

$$-\kappa\triangle u + \mathbf{a}\cdot\nabla u = f, \tag{20}$$

in the unit square with homogeneous Dirichlet boundary conditions and $f(x, y) = 2x\cos(\pi y)$, see [30]. The diffusion coefficient is set to $\kappa = 10^{-2}$, and the advection velocity is $\mathbf{a} = (1, 0)$, thus the global Péclet number is $\mathbf{Pe}_g = \|\mathbf{a}\|/\kappa = 10^2$, see Section 2.

We consider the tensor product spaces of exponential splines of order 4:

$$\mathbb{ES}^4_{\Xi,\boldsymbol{\alpha}} \otimes \mathbb{ES}^4_{\Xi,\boldsymbol{\alpha}}; \tag{21}$$

where $\alpha_j = 5,\ \forall j$, and Ξ as in (18); and the spaces

$$\mathbb{VDQS}^6_{\overline{\Xi},\bar{\boldsymbol{\lambda}}} \otimes \mathbb{VDQS}^6_{\overline{\Xi},\bar{\boldsymbol{\lambda}}}, \tag{22}$$

where the parameters are set $\bar{\lambda}_j = 6,\ \forall j$ and $\overline{\Xi}$ as in (19).

The numerical solutions in (21) and in (22), plotted in Fig. 11 (bottom) for the refinement level with 10 intervals per side, i.e. $h = 0.1$, are stable and allow an accurate representation of the exponential layer at the outflow $x = 1$, without requiring stabilization techniques.

They are compared with the numerical solution in the tensor product space of cubic splines $\mathbb{S}^4_{\Xi} \otimes \mathbb{S}^4_{\Xi}$, see Fig. 13 (top). In this case, without stabilization the solution presents extraneous oscillations (left), instead applying the SUPG formulation (right) the solution is stable but less accurate. We use as the stabilization parameter $\delta = h/(2\|\mathbf{a}\|)$.

4.3. Example 3: problem with discontinuous Dirichlet boundary conditions

The setting for this problem is similar to the previous example ($\kappa = 10^{-2}$, and $\mathbf{a} = (1, 0)$), but in this case we consider $f(x, y) = 0$ and discontinuous Dirichlet boundary conditions as shown in Fig. 12, left.

We consider the approximate solution in spaces (21) with $\alpha_j = 100,\ \forall j$, and in the spaces (22), where the parameters $\bar{\boldsymbol{\lambda}}$ are set as in the 1D problem in Section 4.1, see Table 3. The knot sequences Ξ and $\overline{\Xi}$ are as in (18) and (19) respectively.

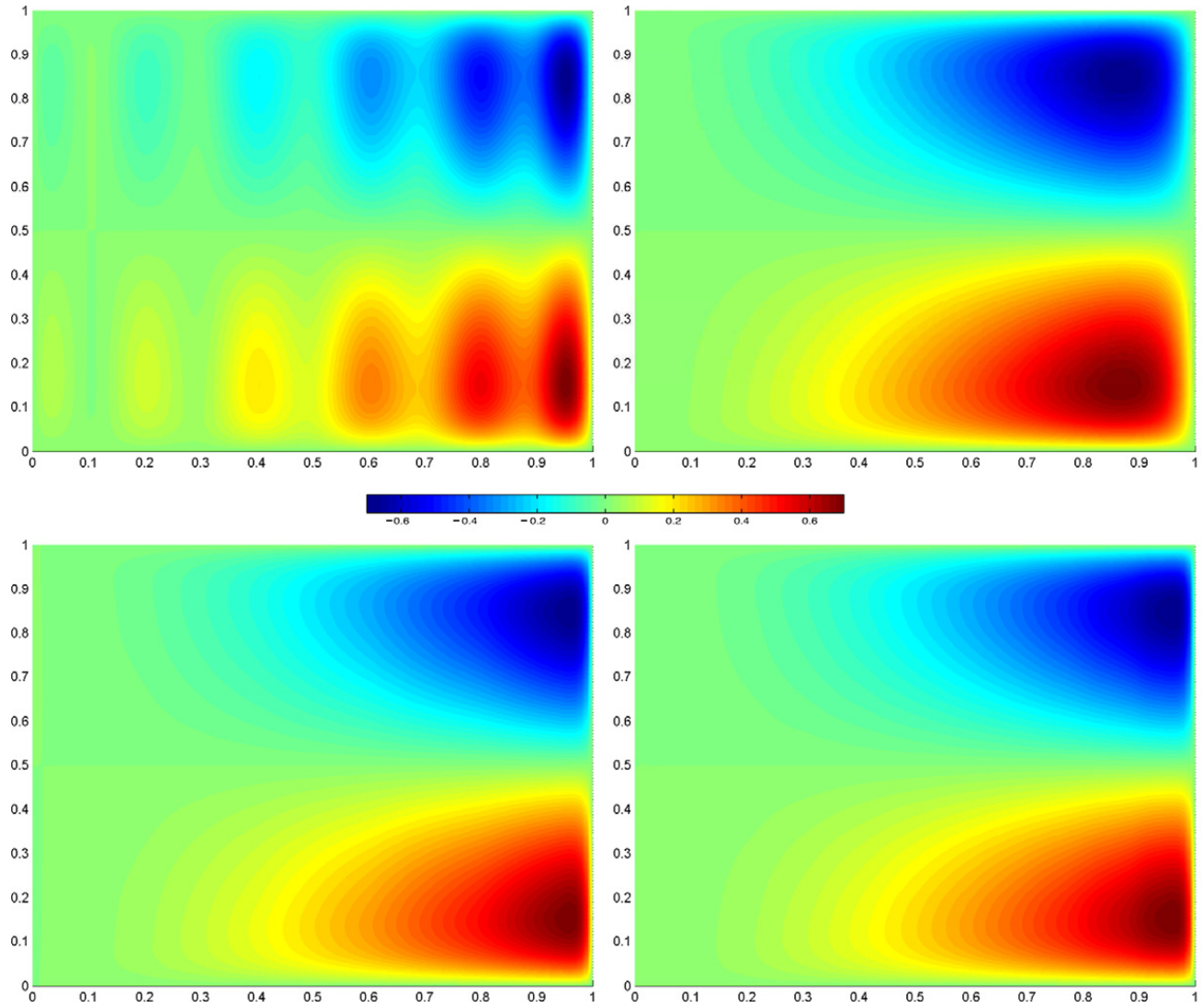

Fig. 11. Example 2. $(X-Y)$ view of the numerical solutions in different spaces. Top: $\mathbb{S}^4_{\Xi} \otimes \mathbb{S}^4_{\Xi}$ without stabilization (left) and with SUPG stabilization (right). Bottom: $\mathbb{ES}^4_{\Xi,\boldsymbol{\alpha}} \otimes \mathbb{ES}^4_{\Xi,\boldsymbol{\alpha}}$ (left) and $\mathbb{VDQS}^6_{\overline{\Xi},\tilde{\lambda}} \otimes \mathbb{VDQS}^6_{\overline{\Xi},\tilde{\lambda}}$ (right) with 10 intervals per side.

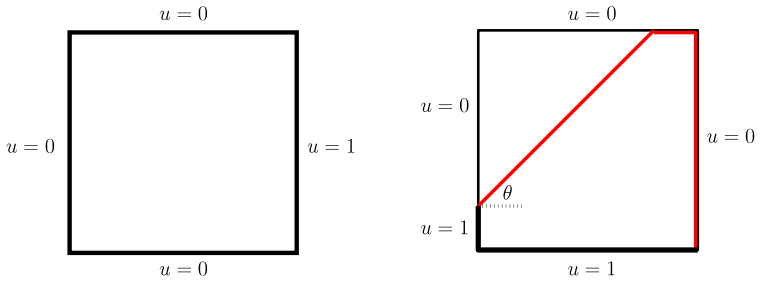

Fig. 12. Left: Example 3, the domain with the boundary conditions. Right: Example 4, the domain with the boundary conditions and sharp layers (red) (For interpretation of the references to colour in this figure legend, the reader is referred to the web version of this article.)

The numerical solutions in (21) and in (22), plotted in Fig. 13 (bottom) for the refinement level with 10 intervals per side, i.e. $h = 0.1$, are stable and accurate without requiring stabilization techniques.

They are compared with the numerical solution in the tensor product space of cubic splines $\mathbb{S}^4_{\Xi} \otimes \mathbb{S}^4_{\Xi}$, see Fig. 13 (top). Even in this case, without stabilization the solution presents extraneous oscillations (left), instead applying the SUPG formulation (right) as in the previous example, the solution is stable but less accurate.

4.4. Example 4: problem with discontinuous boundary conditions and an inner sharp layer

This example is adopted from [6]. We consider the advection–diffusion equation (20) with $f(x, y) = 0$ and discontinuous Dirichlet boundary conditions as shown in Fig. 12, right. The diffusion coefficient is set to $\kappa = 10^{-6}$, and the advection

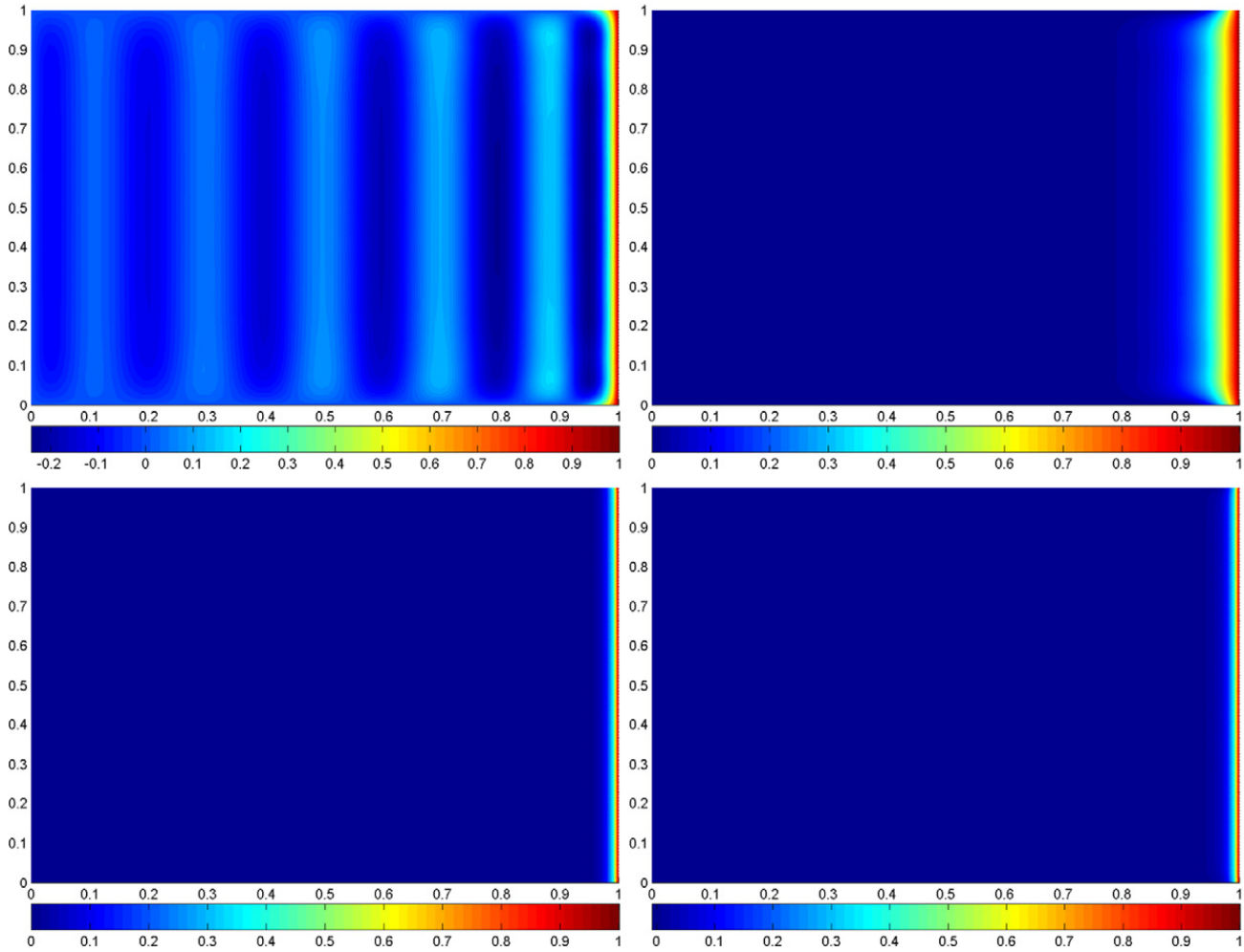

Fig. 13. Example 3. $(X-Y)$ view of the numerical solutions in different spaces. Top: $\mathbb{S}^4_{\Xi} \otimes \mathbb{S}^4_{\Xi}$ without stabilization (left) and with SUPG stabilization (right). Bottom: $\mathbb{ES}^4_{\Xi,\boldsymbol{\alpha}} \otimes \mathbb{ES}^4_{\Xi,\boldsymbol{\alpha}}$ (left) and $\mathbb{VDQS}^6_{\Xi,\bar{\boldsymbol{\lambda}}} \otimes \mathbb{VDQS}^6_{\Xi,\bar{\boldsymbol{\lambda}}}$ (right) with 10 intervals per side.

velocity is $\mathbf{a} = (\cos\theta, \sin\theta)$, thus the global Péclet number, $\mathbf{Pe}_g = \|\mathbf{a}\|/\kappa = 10^6$ is very high. When $\mathbf{Pe}_g$ is greater than one, advection dominates and diffusion is only important in a region of thickness $\mathcal{O}(\mathbf{Pe}_g^{-1} \ln \mathbf{Pe}_g)$ in the outflow boundary layers, [6]. Thus the problem is advection-dominated and sharp layers arise that start at the discontinuity of the boundary condition. We consider the case of $\theta = 45°$.

We look for an approximate solution in the space (22) where the parameters $\bar{\boldsymbol{\lambda}}$ are taken $\bar{\lambda}_j = 7,\ \forall j$ and $\overline{\Xi}$ as in (19).

The boundary conditions are set by using quasi-interpolating schemes on the Dirichlet data in the restriction of the tensor product space at the boundaries. We refer to [10] for a detailed description.

Fig. 14 (top), shows the performance of IgA based on B-splines like functions in (22), compared with classical B-splines IgA. In all tests we consider SUPG formulation with $\delta = h_a/(2\|\mathbf{a}\|)$, see Section 2, where h_a is the element length in the direction of the flow velocity, which in the present example is $h_a = h/\max\{\cos\theta, \sin\theta\}$.

IgA based on classical B-splines requires a high order, $p = 13$, to obtain a stable solution, on a uniform 21×21 grid, see Fig. 14 (top).

In the space (22), for the above mentioned selection of the tension parameters, we obtain a stable solution, see Fig. 14 for two h-refinement steps: uniform 21×21 (center) and 41×41 (bottom) grid, with a very sharp detection of the internal and boundary layers.

According to [6], in Fig. 14 two views are presented for each approximated solution. In the former the solution is sampled with a 21×21 uniform grid and in the latter it is sampled with a 100×100 grid of uniformly distributed points in order to improve the resolution.

We remark that this example is a very challenging test in the context of AD problems, see also [8,9] for comparisons. Both IgA and FEM definitely fail in such a test without a suitable stabilization. Nevertheless, the advantage of (high order NURBS based) stabilized IgA is evident in the good localization of internal and boundary layers and in the elimination of oscillations, see Fig. 14 (top). For comparison, in Fig. 15 we report the solutions obtained with quadratic FEM defined on uniform triangulations. In Fig. 16 we compare, from a rotated point of view, the solution in quadratic FEM spaces with the solution in $\mathbb{VDQS}^{6,}_{\Xi,\bar{\boldsymbol{\lambda}}} \otimes \mathbb{VDQS}^{6}_{\Xi,\bar{\boldsymbol{\lambda}}}$, both defined on the finest level of refinement (3200 triangles and 40 intervals per side).

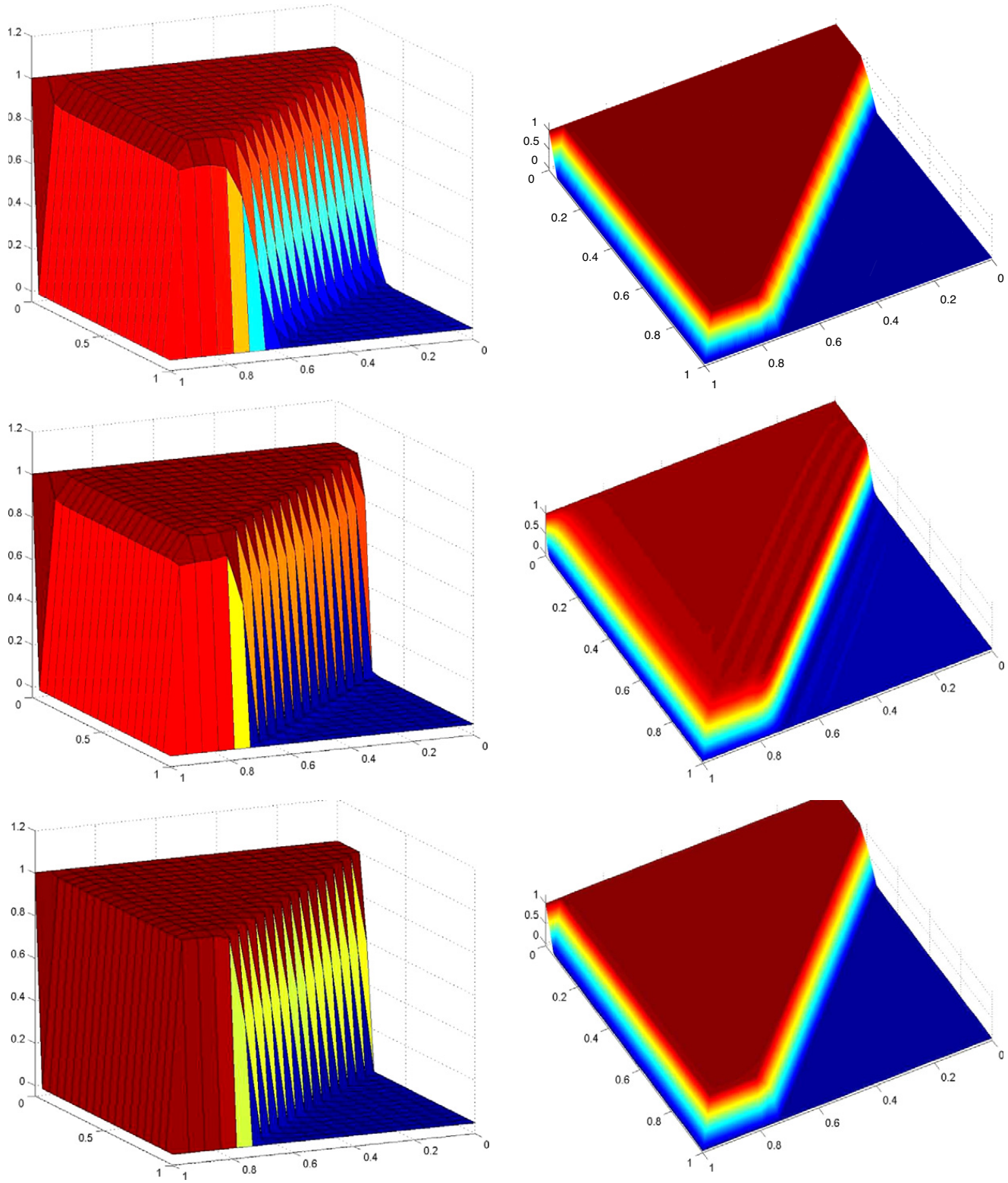

Fig. 14. Example 4. Numerical solutions. Top: $\mathbb{S}_{\overline{S}}^{13} \otimes \mathbb{S}_{\overline{S}}^{13}$. Center/Bottom $\mathbb{VDQS}_{\overline{S},\bar{\lambda}}^{6,} \otimes \mathbb{VDQS}_{\overline{S},\bar{\lambda}}^{6}$ with 20/40 interval per side. Left: 20×20 evaluations. Right: 100×100 evaluations.

Despite the use of SUPG stabilization, the quadratic FEM solution still presents significant overshoots and undershoots about the internal layer and around the $(1, 0)$ corner. The approximated solution obtained by linear FEM has a similar behavior, as can be seen from Table 5 which compares the maximum and minimum values assumed by the solutions obtained in different spaces, all defined on the finest meshes, with the same stabilization.

It turns out that our approach is of interest because it reaches a completely comparable, or even better, quality of the solution as in standard IgA, involving polynomials of significant lower degree and spaces whose computational cost and

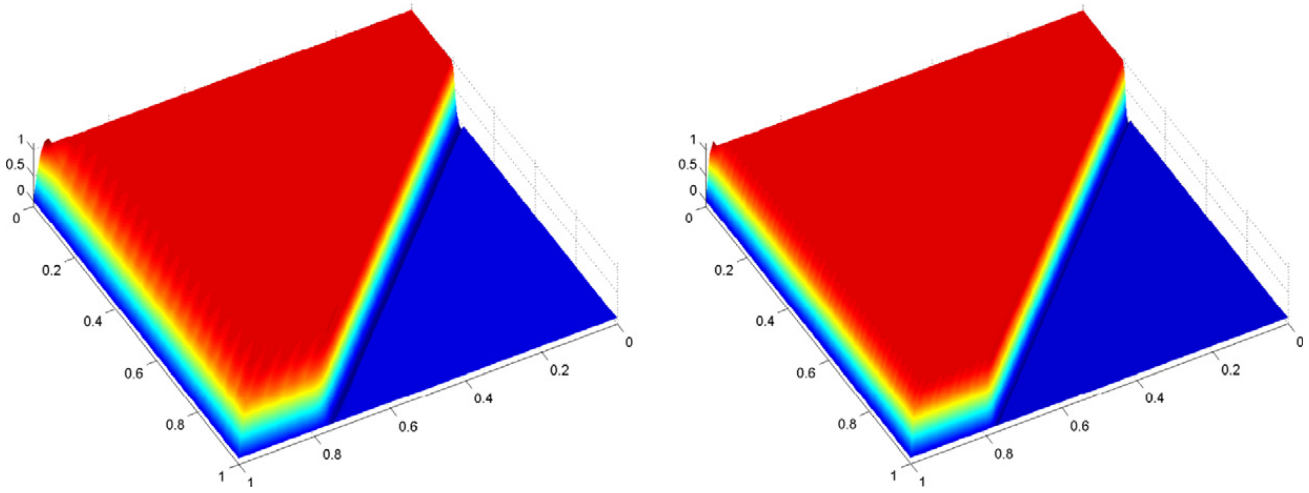

Fig. 15. Example 4. Numerical solutions with SUPG quadratic FEM defined on uniform three directional meshes with 800 (left) and 3200 (right) triangles.

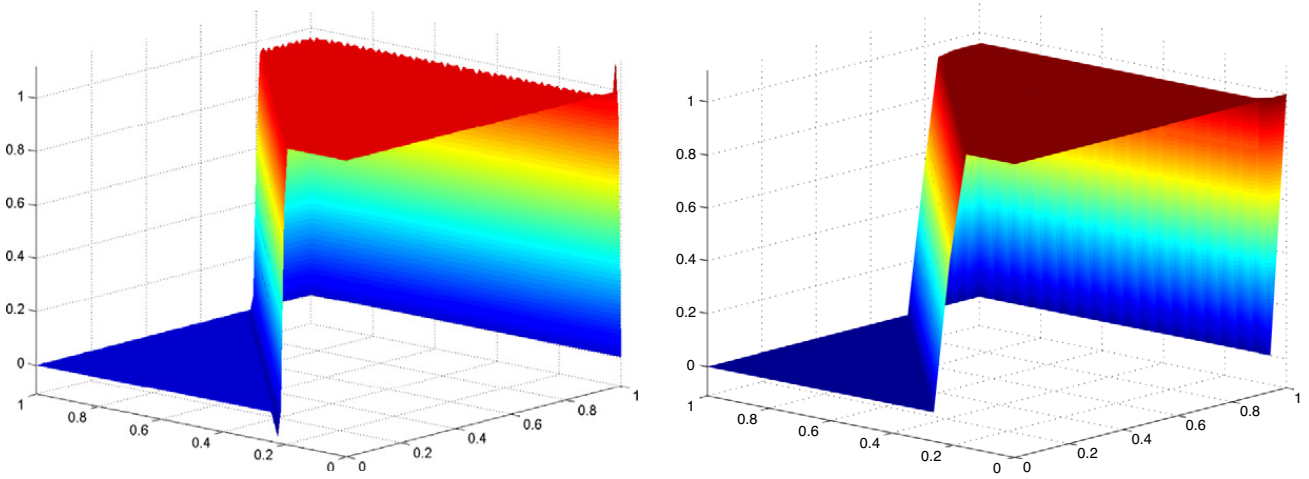

Fig. 16. Example 4. From a rotated point of view the solutions with quadratic FEM (left) and with $\mathbb{VDQS}^{6,}_{\Xi,\tilde{\lambda}} \otimes \mathbb{VDQS}^{6}_{\Xi,\tilde{\lambda}}$ (right) both at the finest level of refinement.

Table 5
Example 4. Maximum and minimum values for the solutions of (20) with linear/quadratic FEM (12,800/3200 triangles), tensor product of order 13-B-splines (21×21 grid) and $\mathbb{VDQS}^{6,}_{\Xi,\tilde{\lambda}} \otimes \mathbb{VDQS}^{6}_{\Xi,\tilde{\lambda}}$ (41×41 grid).

	FEM $\mathbb{P}_2$	FEM $\mathbb{P}_3$	$\mathbb{S}^{13}_{\Xi} \otimes \mathbb{S}^{13}_{\Xi}$	$\mathbb{VDQS}^{6,}_{\Xi,\tilde{\lambda}} \otimes \mathbb{VDQS}^{6}_{\Xi,\tilde{\lambda}}$
max	1.199	1.203	1.0003	1.0035
min	−0.010	−0.123	−0.0002	−0.0012

condition number[8] of the corresponding system are comparable to classical quintics (see Section 4.1 for the one dimensional case).

5. Conclusion

The ability of exponential and variable degree splines to properly describe sharp variations is well known in the context of shape-preserving interpolation and approximation.

Thanks to this property, isogeometric analysis based on exponential or variable degree B-splines results in an efficient paradigm to face advection–diffusion problems with the advection dominating part. The key ingredient of such an approach is the use of Galerkin approximating spaces with high smoothness, as in IgA based on classical B-splines or NURBS, but

8 Referring to Table 5, the condition number for the space $\mathbb{S}^{13}_{\Xi} \otimes \mathbb{S}^{13}_{\Xi}$ is about 10^{10}, whereas for $\mathbb{VDQS}^{6,}_{\Xi,\tilde{\lambda}} \otimes \mathbb{VDQS}^{6}_{\Xi,\tilde{\lambda}}$ is only about 600.

particularly well suited to describe sharp layers involving very strong gradients. This produces a significant reduction of extraneous oscillations which are typical for polynomial-based finite elements. For some test problems, this reduction is so significant that it eliminates the need of any stabilization.

Variable degree B-splines are more attractive than exponential B-splines for their polynomial structure, which results in a lower computational cost, and because they possess a simple stable geometric construction completely analogous to classical polynomial B-splines. Explicit simple strategies have been presented to select the tension parameters for variable degree spline spaces so that they mimic the behavior and features of the corresponding spaces of exponential splines.

In particular, IgA based on variable degree splines reaches a completely comparable, or even better, quality of the solutions as standard B-splines based IgA, by using suitable (piecewise) polynomial spaces of significant lower degree, which are isomorphic to standard cubics or quintics.

Acknowledgments

The authors would like to thank the anonymous referees for their useful comments.

References

[1] A.N. Brooks, T.J.R. Hughes, Streamline upwind/PetrovGalerkin formulations for convection dominated flows with particular emphasis on the incompressible NavierStokes equations, Comput. Methods Appl. Mech. Engrg. 32 (1982) 199–259.
[2] L.P. Franca, S.L. Frey, T.J.R. Hughes, Stabilized finite element methods: I. Application to the advective–diffusive model, Comput. Methods Appl. Mech. Engrg. 95 (1992) 253–276.
[3] L.P. Franca, G. Hauke, A. Masud, Stabilized finite element methods, in: Finite Element Methods: 1970s and Beyond, CIMNE, Barcelona, 2003 (Chapter 3).
[4] M.-C. Hsu, Y. Bazilevs, V.M. Calo, T.E. Tezduyar, T.J.R. Hughes, Improving stability of stabilized and multiscale formulations in flow simulations at small time steps, Comput. Methods Appl. Mech. Engrg. 199 (2010) 828–840.
[5] T.J.R. Hughes, L.P. Franca, G.M. Hulbert, A new finite element formulation for computational fluid dynamics: VIII. The Galerkin/least-squares method for advective–diffusive equations, Comput. Methods Appl. Mech. Engrg. 73 (1989) 173–189.
[6] T.J.R. Hughes, J.A. Cottrell, Y. Bazilevs, Isogeometric analysis: CAD, finite elements, NURBS, exact geometry and mesh refinement, Comput. Methods Appl. Mech. Engrg. 194 (2005) 4135–4195.
[7] Y. Bazilevs, L. Beirao, Da Veiga, J.A. Cottrell, T.J.R. Hughes, G. Sangalli, Isogeometric analysis: approximation, stability and error estimates for *h*-refined meshes, Math. Models Methods Appl. Sci. 16 (2006) 1031–1090.
[8] Y. Bazilevs, V.M. Calo, J.A. Cottrell, J.A. Evans, T.J.R. Hughes, S. Lipton, M.A. Scott, T.W Sederberg, Isogeometric analysis using T-splines, Comput. Methods Appl. Mech. Engrg. 199 (2010) 229–263.
[9] M. Dörfel, Simeon B. Jüttler, Adaptive isogeometric analysis by local h-refnement with T-splines, Comput. Methods Appl. Mech. Engrg. 199 (2010) 264–275.
[10] P. Costantini, C. Manni, F. Pelosi, M.L. Sampoli, Quasi-interpolation in isogeometric analysis based on generalized B-splines, Comput. Aided Geom. Design 27 (2010) 656–668.
[11] A. Quarteroni, Numerical Models for Differential Problems, Springer, 2009.
[12] C. Manni, F. Pelosi, M.L. Sampoli, Generalized B-splines as a tool in isogeometric analysis, Comput. Methods Appl. Mech. Engrg. (2010) doi:10.1016/j.cma.2010.10.010. online.
[13] P. Costantini, T. Lyche, C. Manni, On a class of weak Tchebycheff systems, Numer. Math. 101 (2005) 333–354.
[14] L.L. Schumaker, Spline Functions: Basic Theory, third edition, Cambridge U.P., 2007.
[15] P. Costantini, Curve and surface construction using variable degree polynomial splines, Comput. Aided Geom. Design 17 (2000) 419–446.
[16] P. Costantini, C. Manni, Shape-preserving C^3 interpolation: the curve case, Adv. Comput. Math. 18 (2003) 41–63.
[17] P.E. Koch, T. Lyche, Interpolation with exponential B-splines in tension, in: G. Farin, et al. (Eds.), Geometric Modelling, in: Computing Suppl., vol. 8, Springer-Verlag, 1993, pp. 173–190.
[18] B.I. Kvasov, P. Sattayatham, GB-splines of arbitrary order, J. Comput. Appl. Math. 104 (1999) 63–88.
[19] M.L. Mazure, Chebyshev–Bernstein bases, Comput. Aided Geom. Design 16 (1999) 649–669.
[20] G. Wang, M. Fang, Unified and extended form of three types of splines, J. Comput. Appl. Math. 216 (2008) 498–508.
[21] M. Marušic, M. Rogina, Sharp error bounds for interpolating splines in tension, J. Comput. Appl. Math. 61 (1995) 205–223.
[22] C. de Boor, A Practical Guide to Spline, Revised ed., Springer, 2001.
[23] D.G. Schweikert, An interpolation curve using a spline in tension, J. Math. Phys. 45 (1966) 312–317.
[24] P. Costantini, F. Pelosi, M.L. Sampoli, Boolean surfaces with shape constraints, Comput. Aided Des. 40 (2008) 62–75.
[25] P. Costantini, C. Manni, Geometric construction of generalized cubic splines, Rend. Mat. Appl. 26 (2006) 327–338.
[26] P. Costantini, F. Pelosi, Shape-preserving approximation of spatial data, Adv. Comput. Math. 20 (2004) 25–51.
[27] N. Dyn, D. Levin, A. Luzzatto, Exponentials reproducing subdivision schemes, Found. Comput. Math. 3 (2003) 187–206.
[28] L.L. Schumaker, G.W. Reddien, On a collocation method for singular twopoint boundary value problems, Numer. Math. 25 (1976) 427–432.
[29] P. Costantini, Properties and applications of new polynomial spaces, Int. J. Wavel., Multir. Infor. Proc. 4 (2006) 489–507.
[30] G. Sangalli, A robust a-posteriori estimator for advection–diffusion–reaction problems, Math. Comput. 77 (2008) 41–70.